National Cheng Kung University

Institute of Space and Plasma Sciences

2020 Annual Report

研究生 ： 林彥呈 Yen-Cheng Lin

指導教授 ： 張博宇 Po-Yu Chang

Contents

List of Figures

1 Abstract

This report summarizes the works content in 2020, mainly the completion of the experiment of the mini-Marx system, the experiment of testing the plasma jet, and the work of developing the x-ray pinhole camera. The experiment of the mini-Marx system is for testing the performance of the mini-Marx system made by the other research team. The output voltage of the mini-Marx system has been measured, the result is -12.99±0.04 kV and will be discussed in section 2. For the plasma-jet experiment, the new conical-wire array has been designed and the images of the plasma jets generated by the twisted-conical-wire arrays with different twisted angles were taken. The hollow region due to the force balance between centrifugal force and the pressure of the incoming plasma was found in the images. Finally, for the x-ray pinhole camera, the pinhole camera and the control box have been assembled and the LabVIEW code for controling the pinhole camera have been written. However, the x-ray pinhole camera still has some problems to be solved.

3 Plasma jet

In our research, we want to generate a plasma jet and study physics in the plasma jet. Futher, we would like to use the plasma flow for studying phenomena in space. To generate plasma jets, we use conical-wire arrays driven by the pulsed-power system we built . Figure 8 is the principle of the plasma jet formation[2]. In step 1, the high current goes through the wires from the top to the bottom. The current heats and ionizes the wires into the plasma through ohmic heating. After that, the plasma is pushed by the JxB force and accumulates on the axis forming a precursor. Third, the plasma jet is formed by the nonuniform z-pinch effect due to the radius difference between the top and the bottom of the array.

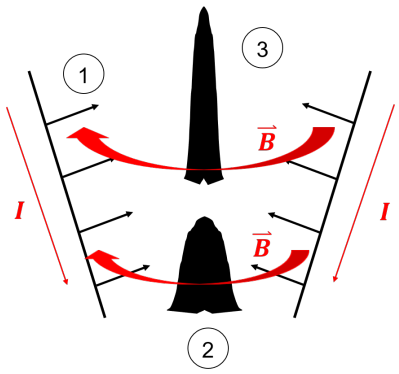

Figure 8: The principle of the plasma jet formation.

Figure 9(a) is the section view of the old design of the conical-wire array. The figure 9(b) is the photo of the old design of the conical-wire array. In the old design of the conical-wire array, the field of view was blocked by the top wire support. Further, it was not easy to install the conical-wire array. Figure 9(c) is the photo of the discharge taken by a camera. The exposure condition was: f/22 in f-number, 120 mm in focus length, "low level 1" in ISO setting, 20 s in exposure time. The region of the plasma jet was overexposed. In order to solve the problems encountered in the old design of the wire array and the problem of overexposure, we had a new design of the wire array and a filter was added in front of the camera.

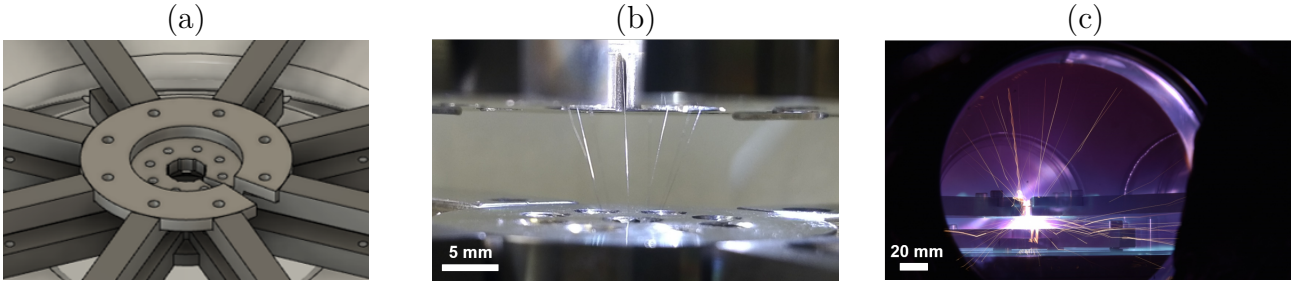

Figure 9: (a) The section view of the conical-wire array. (b) The conical-wire array. (c) The figure of the discharge.

3.1 New design of the conical-wire array

To fix the problem of the field of view being blocked, we designed a new way to hold the conical-wire array. Figure 10(a) is the new design of the conical-wire array. The top wire support is changed from a round disk to four independent supports. Each support can be disassembled and assembled independently, shortening the assembly time and improving the ease of assembly. Moreover, it provides a much better field of view. The drawing of the new conical-wire array is provided in Appendix 7.1. Figure 10(b) is the section view of the new conical-wire array. The array has an inclination angle α of 30° with respect to the axis. The array consists of 4 Tungsten wires with a diameter of 20 μm. Figure 10(c) is the photo of the actual conical-wire array.

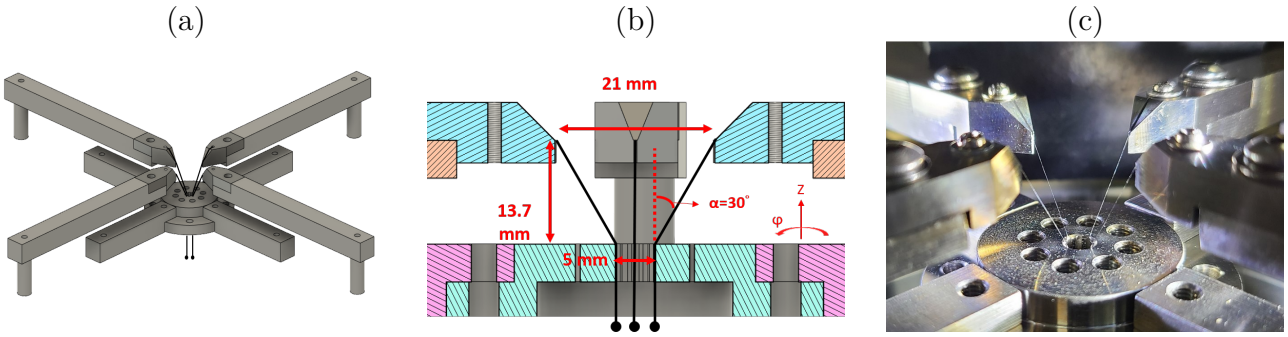

Figure 10: (a) The new design of the conical-wire array. (b) The section view of the new conical-wire array. (c) The new conical-wire array.

In the research, we also studied the rotational plasma jets. To generate the rotational plasma jets, the conical-wire array was twisted. Figure 11 shows images of wire arrays with different twisted angle. The (a) series is the schematic diagrams of the wire arrays. The red dots represent the contact points of the wires at the bottom, and the blue dots represent the contact points of the wires at the top. In the non-rotation case, the center of the disk, red dots

and the corresponding blue dots are aligned. In the twisted case, the wire has a twist angle θ as the mark in the figure. The top of the array was rotated clockwise or counterclockwise with respect to the bottom of the array leading to a conical-wire array twisted in counterclockwise or clockwise direction,respectively. The result of the plasma jet will be discussed in section 3.3.

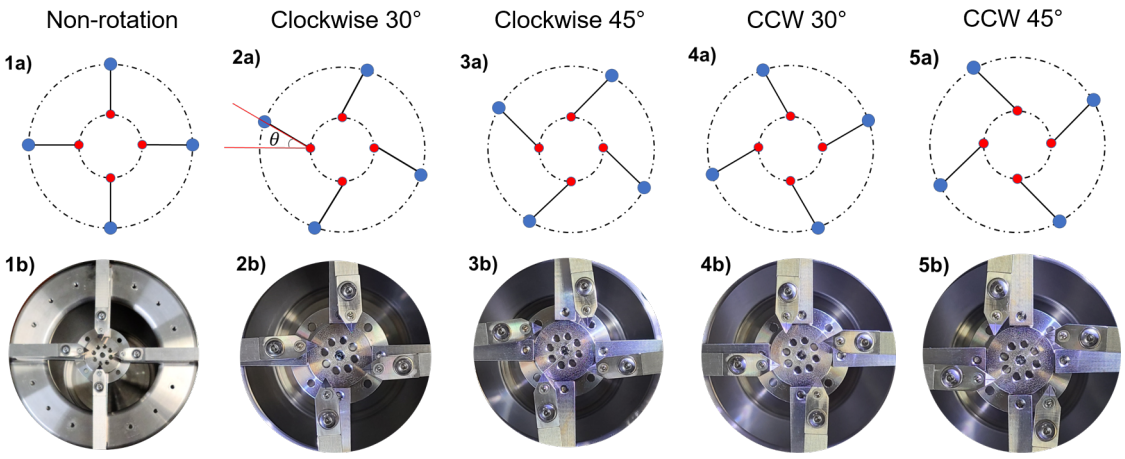

Figure 11: Images of wire arrays with different twisted angle. (1a~5a) Schematic diagrams. (1b~5b) Actual structures.

The new design of the conical-wire array still had some problems. In the twisted case, the conical-wire array was rotated with a twist angle. The inclination angle would change because of the rotation. In the 30-degree case, the inclination angle would change to 38.75 degree since the diameter of the top of the conical-wire arrays changes due to the rotation as shown in the following. Figure 12(a) is the top view of the schematic diagram of the conical-wire array. The blue line is the top wire support. When the top wire support is rotated 30 degrees, in order to maintain the same inclination angle, the length of the top wire support needs to be adjusted. The black line represents the new length of the top wire support. The X parameter is the length difference that needs to be adjusted. Figure 12(b) is the table of the length difference with different twist angles. In the 30-degree case, 1.5 mm needs to be added to the length of the top wire support to maintain the same inclination angle. To solve this problem, 3rd edition of the conical-wire array was designed. Figure12(c) is the CAD drawing of the new wire-array support. The left-hand side is the previous design of the wire array support while the right-hand side is the new wire array support. The original through-hole with a diameter of 4.5 mm was modified into a long strip, which allows the support to move. So the length of the top wire support can be adjusted. The CAD drawing of the new conical-wire array is given in Appendix 7.1.

(a)

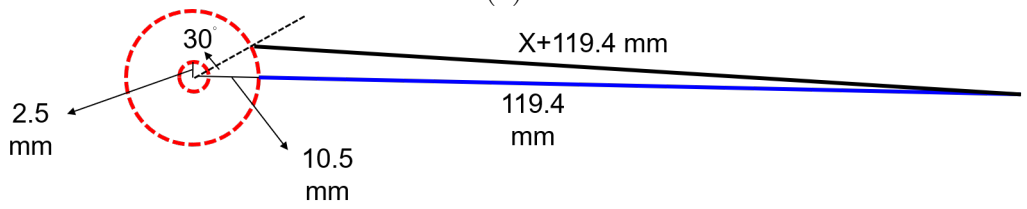

(b)

Twisted angle	Total length	Length different
0	119.4	0
15	119.8	0.39
30	120.9	1.52
45	122.7	3.30
60	125.0	5.58

(c)

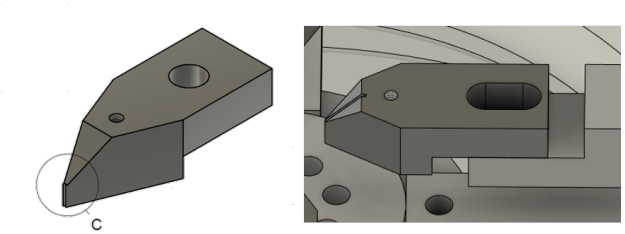

Figure 12: (a) The schematic diagram of the conical-wire array. (b) The table of the length different with different twisted angle. (c) The CAD drawing of the new wire array support.

3.2 Cellophane

In figure9(c), the image of the plasma jet was overexposed. To solve this problem, we used cellophane as an neutral density (ND) filter. We measured the ND power of the cellophane. Figure 13(a) is the experimental setup of the measurement. We used a flashlight as a continuous light source. In front of the flashlight, different numbers of layers of cellophane will reduce the light intensity differently. In the experiment, the number of layers was the experimental variable. The photodiode detector (Thorlabs, DET10 A/M) measured the light intensity before and after the light penetrates the cellophane and gave the result in voltages. Figure 13(b) is the result of the cellophane attenuation ability. The x-axis represents the light intensity before the light penetrates the cellophane. The y-axis represents the light intensity after the light penetrates the cellophane. In the figure, the black circles, blue triangles, and pink squares represent data with numbers of layers of cellophane from one to three, respectively. From the slopes of the fitting lines, the light intensity after the light penetrates one-layer of cellophane will only have 8 % of the light goimg through the cellophane, while only 2 % and 1 % of the light was retained through two- and three-layers of cellophane, respectively.

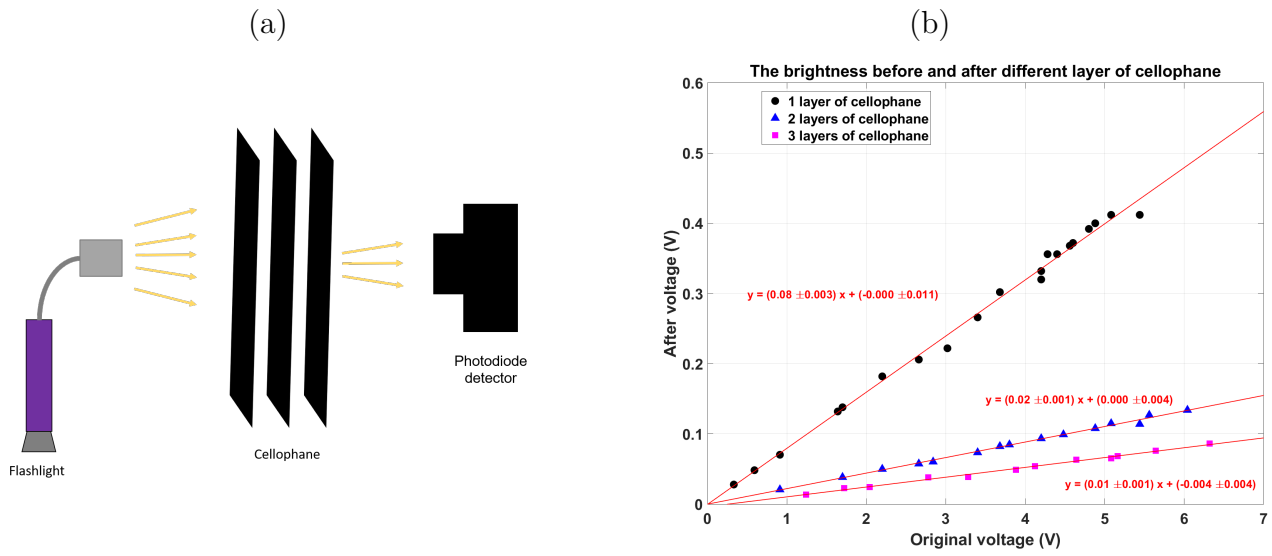

Figure 13: (a) The experimental setup of the cellophane testing. (b) The result of the cellophane attenuation ability.

Table 2(a) is the table of parameters of ND filters. For example, the ND-100 filter attenuates the light intensity to 1% from the table,. Comparing the experimental result and the table of parameters of the ND filters, the attenuation ability of the three-layer cellophane is the same as ND-100 filter. The attenuation of the two-layer cellophane is between ND-30 and ND-64 filter. The attenuation ability of one-layer cellophane is between the ND-8 and ND-16 filter. Table 3(b) is the table of the ND number with different number of layers of cellophane.

Table 2: The parameter of the ND filter.

ND number	Fractional transmittance
8	12.5%
16	6.25%
32	3.125%
64	1.563%
100	1%

Table 3: The different number of layer of cellophane.

Layer #/	ND number
1 layer	12.5
2 layer	50
3 layer	100

3.3 Plasma jet

To observe the plasma jet, we used the camera to take photos from the side and from the top. Figure 14 is the experimental setup. The camera is marked as Camera 1 and Camera 2 in the figure. Table 4 lists the parameters of the camera.

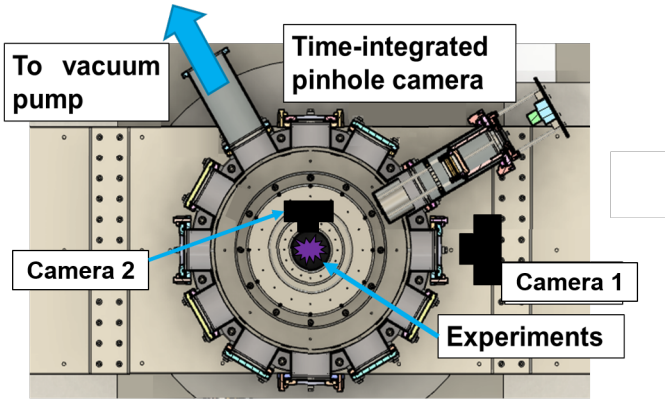

Figure 14: The experiment setup.

Camera	Nikon D750
Aperture	f/22
Focal length	120 mm
ISO	Low Level
Shutter	20 s
Filter	ND64 (for the side) ND100 (for the top)

Table 4: The parameter of the camera.

Figure 15 shows time-integrated images of plasma jets taken from the side. Each twist angle is marked above each image. Figure 16 is the profile of the plasma jet at the center from the bottom to the top (from point A to point B). Since the field of view for twisted conical-wire array was blocked with twisted angles in CCW, the data from those shots was not discussed. In the system, the magnetic field has two components. The magnetic field in the azimuthal direction φ provides the JxB force to compress the plasma jet. It is caculated as follow:

$$B_\varphi = \frac{\mu_0 I}{2\pi r}\cos\alpha \tag{3}$$

where r is the averaged radius of the wire array, α is the inclination angle of the wire array. On the other hand, the current has the φ component in the twisted-conical-wire array. Therefore,

the magnetic field would have the component in the z-direction. The magnetic field in the z-direction is as follow:

$$B_z = \frac{\mu_0 I}{2\pi r} \sin\theta \cdot \sin\alpha \tag{4}$$

where θ is the twist angle of the wire array. The current multiply $\sin\theta$ first to project to the r-φ axia, and times $\sin\alpha$ to project to the φ axia. The magnetic field in the z-direction may inhibit the thermal conduction losses. The temperature of the plasma jet may be higher leading to a brighter emission. From the profile, the 45-degree case was darker than the non-twisted and 30-degree cases. It is potentially because the compression is less efficient with the twisted angle 45° leading to less emissions. The 30-degree case was brighter than the non-twisted case potentially because the magnetic field in the z-direction of the twisted angle 30° was potentially larger than that in the non-twisted case. Therefore, the plasma jet was brighter than the original one.

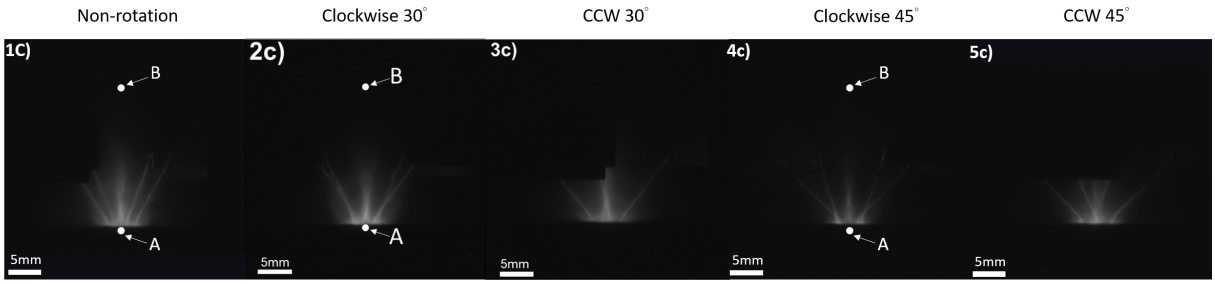

Figure 15: Time-integrated images from the side view.

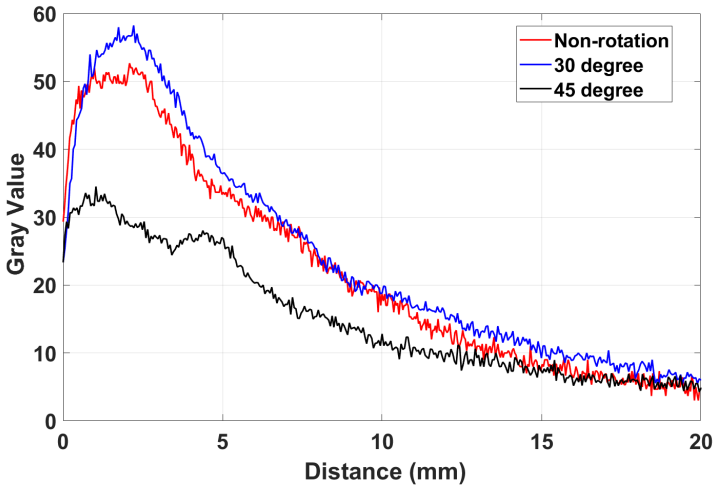

Figure 16: The profile of the plasma jet at the center from the bottom to the top (A to B).

Figure 17 is the time-integrated images of the plasma jet taken from the top view. Each twisted angle is marked above each image. Figure 18 is the profile of the plasma jet from the

top view (from point C to point D). The hollow region at the center with the twisted angle 30 degree in clockwise and counterclockwise was due to the force balance between centrifugal force and the pressure of the incoming plasma. It also shows that the angular momentum of the plasma flow was conserved in the system[3].

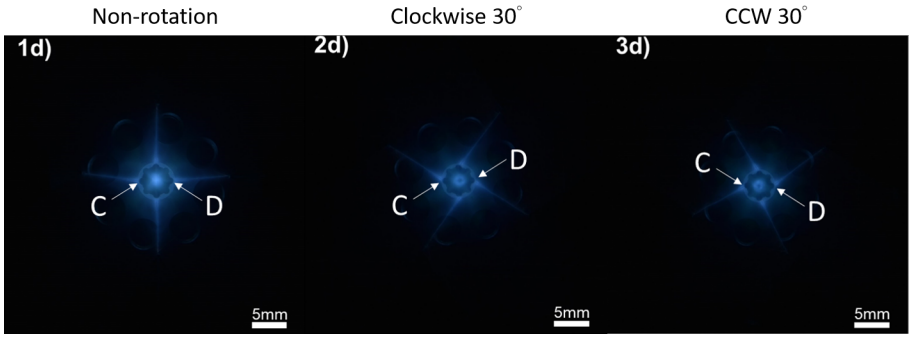

Figure 17: Time-integrated images from the top view.

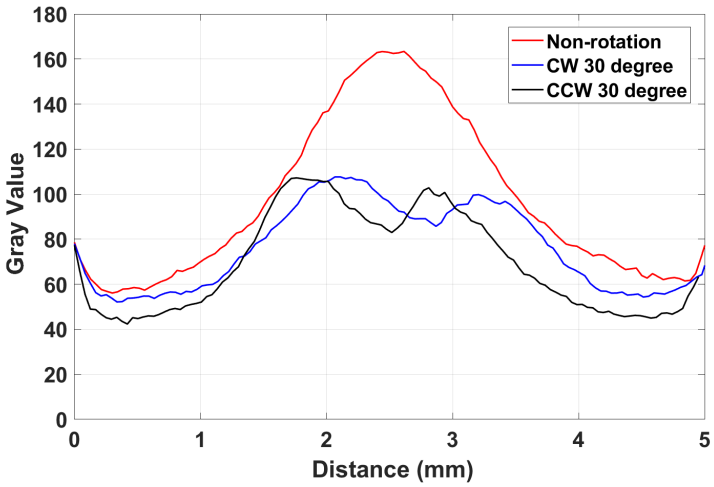

Figure 18: The profile of the plasma jet from the top view (C to D).

To measure the radius of the hollow region, the center of the hollow region was marked by using Matlab. First, the image was turned into a grayscale image as show in Figure 19(a). After that, the grayscale image was converted into the black and white image by using the threshold number 0.315 in the function im2bw. Therefore, the center hollow region with a sharp edge was obtained. Afterward, the circle function $x^2 + y^2 = r^2$ was used to fit the edge. The center of the hollow region would be obtained from the fitted equation. The fitted circle is shown in Figure 19(a), while the fitted edge is shown in Figure 19(b) with red line. After we got the center point, profiles of different orientations through the center point were taken. Lines of different profiles are shown in Figure 19(a).

Figure 19: (a) The grayscale image of the plasma jet front the top view. (b) The threshold scale image of the plasma jet front the top view.

Figure 20 is one of the profiles of the plasma jet. It shows that the center of the plasma jet is darker than the surroundings. Two Gaussian functions were fitted to the two-peak profile. Then, the diameter of the hollow region was defined as the distance between two peaks. Profiles at 0, 45, 90, and 135 degrees were obtained. The diameter of the hollow region was 1.05±0.03 mm with twisted angle of 30 degree in the clockwise direction, and 1.02±0.04 with twisted angle of 30 degree in the counterclockwise direction. They are the same meaning that the angular momentums have the same amplitude in two cases.

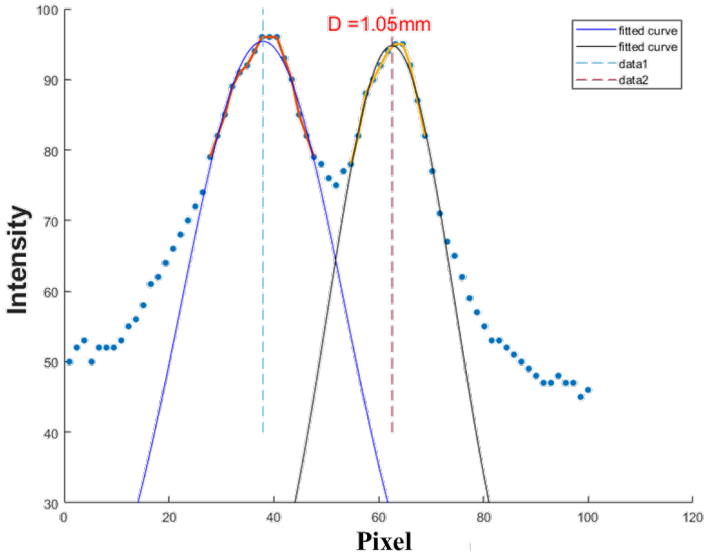

Figure 20: One of the profile of the plasma jet.

3.4 Discussion

So far, we only have time-integrated images. To understand the physical mechanism of the plasma jet from the picture is very limited because all details from different time are stacked on top of each other in the same image. We need to develop time-resolved imaging system.

Alternatively, images of plasma jets will be taken by the gated x-ray pinhole camera in the future. The physics of the plasma jet generated by the twisted-conical-wire array will also be studied with time-resolved measurements in densities, temperatures, and magnetic fields.

4 X-ray pinhole camera

In order to observe the plasma jet and study its physics, the x-ray pinhole camera is used to take the time-integrated image of the plasma jet. Figure 21 is the flow chart of the pinhole camera. The x-ray generated by the plasma jet will pass through the pinhole and project on the photocathode emitting electrons. The accelerate grid is connected to the ground while the photocathode was connected to a negative voltage. Therefore, electrons are accelerated by the accelerate grid. When electrons arrive the micro-channel plate (MCP) set, the number of the electrons are multiplied by up to 10^7 by the MCP set where a DC high voltage is applied across the MCP. After the MCP set, electrons hit the fluorescent screen in the backside of the MCP. Finally, the screen emits visible light which is captured by a CMOS camera.

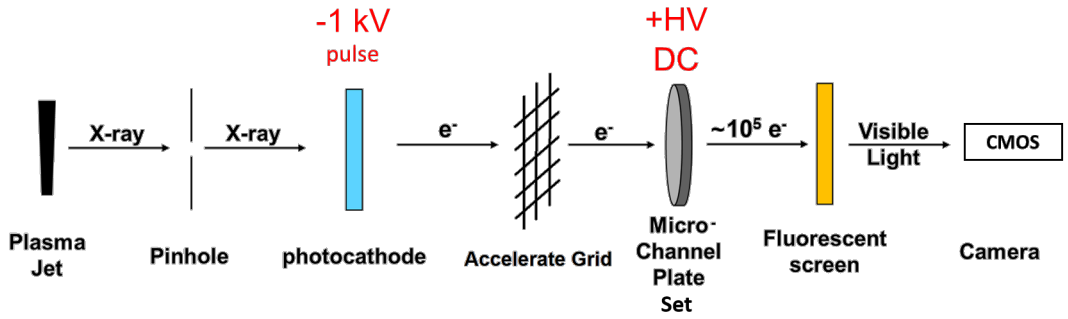

Figure 21: The flow chart of the pinhole camera.

4.1 MCP testing

In order to confirm that the MCP set works properly, we first use the heated filament to provide electrons and test the function of the accelerate grid and the MCP set. The MCP set consists of two MCP plates and the fluorescent screen. Each part has a connecting wire. Figure 22(a) is the screenshot of the design diagram of the MCP set. There are three connecting wires. The MCP_1 input is for connecting with the ground, the MCP_2 output is for connecting with voltage supply, and the screen is for screen voltage supply. Figure 22(b) is the figure of the MCP viewed from the fluorescent screen. The three metal wires are the voltage-supply wires described above.

(a) (b)

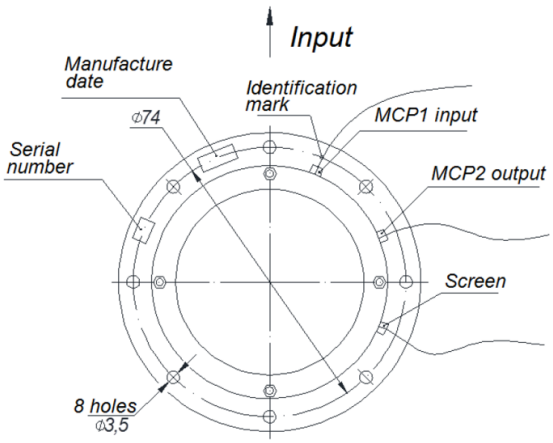

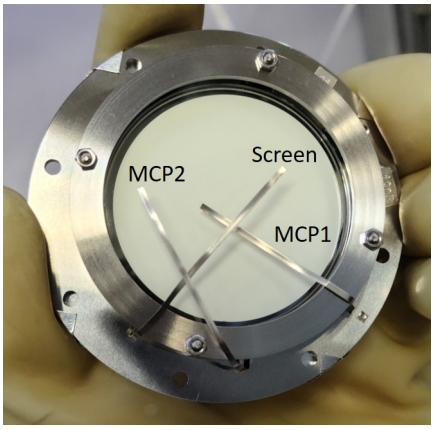

Figure 22: (a) The design diagram of the MCP. (b) The figure of thge MCP from the fluorescent screen view.

Figure 23(a) is the photo of the MCP assembly. The connecting wires of the MCP had been connected to the Miniature High Voltage (MHV) feed through at the top flange of the x-ray pinhole camera. Figure 23(b) is the heated filament used in testing the MCP. The filament was connected to the DC-DC converter and a resistor. The DC-DC converter was for providing the volatge to heat the filament. The ground of the DC-DC converter is stepped up to a negative high voltage supplied by a power supply. Therefore, there is an electric field between the filament and the accelerate grid so that electrons are accelerated toward the grid. The resistor was for limiting the current going through the filament. The resistor was 2-ohm and the current was about 1.65 A. During the testing, the chamber of the pinhole camera was pumped down to 10^{-6} Torr.

(a) (b)

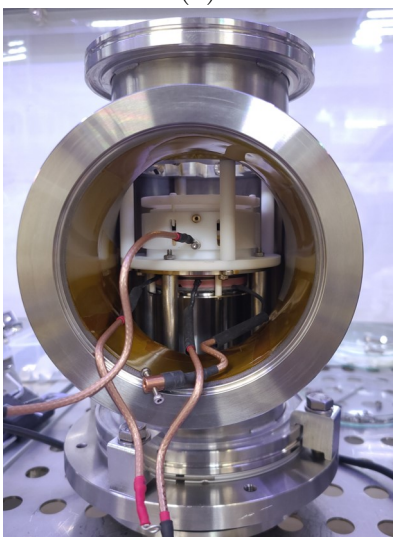

Figure 23: (a) The figure of testing MCP. (b) The filament used in the testing MCP.

Figure 24(a) is the circuit of testing the MCP. The high-voltage power supply was connected through the resistor to limit the current. Two resistors were connected between the screen and two MCP paltes in the MCP set to divide the voltage. Therefore, only one power supply is needed. Figure 24(b) is the result of testing the flurescent screen. The green light was the emitted visible light from the electrons hitting the fluorescent screen. The HVPs provided a high voltage up to 5.7 kV. The working voltage of the screen was 2.8~4.4 kV, and the corresponding working voltage of the MCP_2 was 1.4~2.2 kV. After testing, the pinhole camera has been successfully assembled and installed in the system.

(a) (b)

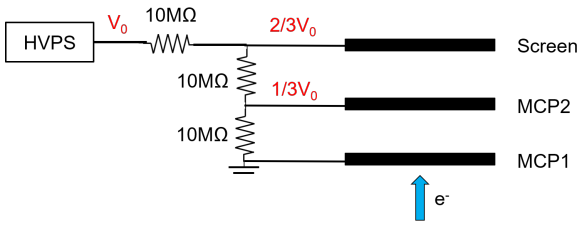

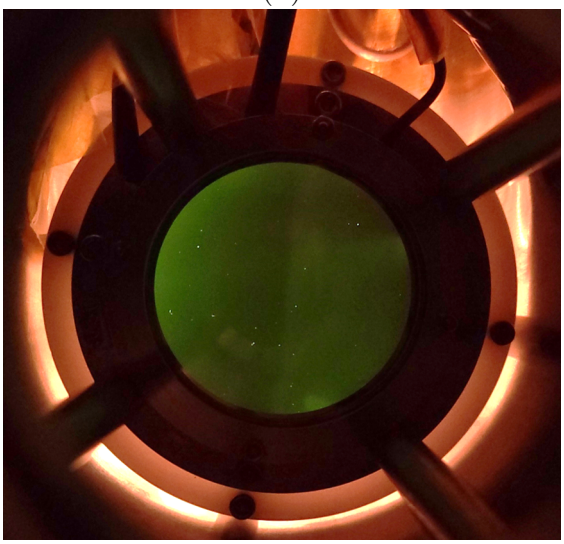

Figure 24: (a) The circuit of the testing MCP. (b) The flurescent screen.

4.2 The pinhole camera control box

The pinhole camera control box is for controlling the exposure time of the pinhole camera and triggering the pinhole camera. The control box can supply the DC high-voltage around 4 kV for the MCP set, and provide a negative high voltage pulse for the photocathode.

4.2.1 Negative high-voltage pulse

The negative high-voltage pulse is the signal to control the exposure time. The amplitude of the negative high-voltage pulse is 1 kV and the width is 1 μs. Figure 25(a) is the circuit of the negative high-voltage pulse generator. The circuit was built based on one stage of a Marx generator. The switch of the Marx generator is the MOSFET SCT3160KL, and the MOSFET is controlled by the driver IC FOD3184. To control the switch, the 20-V pulse signal will be

sent to the MOSFET (M_1). The switch will be closed when the pulse signal is high. In the meantime, the drain (D) pin of M_1 is connecting to the source (S) pin, and the output voltage of the high-voltage pulse generator drops to the negative high voltage. When the 20-V pulse signal is low, the switch will be opened, the D pin of M_1 supposes to be disconnected from the S pin, and the output voltage supposes to change back to zero. However, the output voltage doesn't change back to zero as expected. Therefore, another MOSFET (M_2) is used to force the output of the high-voltage pulse generator connected to the ground. To control M_2, a second 20-V signal pulse with a delay is needed. Figure 25(b) is the time relation of the pulses. The width of the negative high voltage pulse is controlled by the delay time between the input signal 1 and 2. The output pulse drops to the negative voltage at time A, and changes back to the ground at time C.

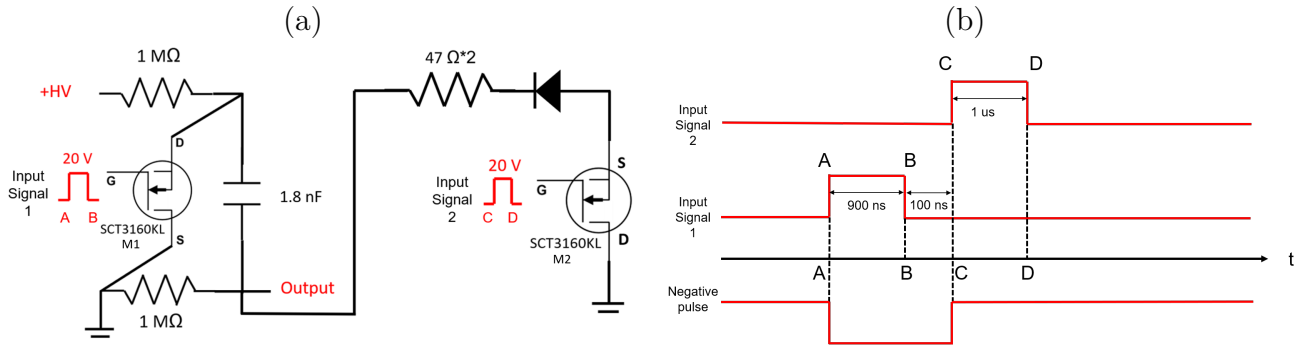

Figure 25: (a) The circuit of the negative high voltage pulse generator. (b) The time relation of the pulse.

To generate two input signals with a specific time difference in between, we use the delay IC DS1023-500. The delay IC reproduces the logic state of the input after a delay determined by the state of the eight input pins P0 - P7. The 8-bit digital signal was generated by the Arduino Mega. Figure 26(a) is the pin definitions of the delay IC. The delay IC has the smallest delay time in 50 ns, and the max delay time in 1325 ns. Figure 26(b) is the result of the delay IC. The red line is the input signal and the blue line is the output signal. These two signals have a delay time of 503 ns when the delay was set at 490 ns.

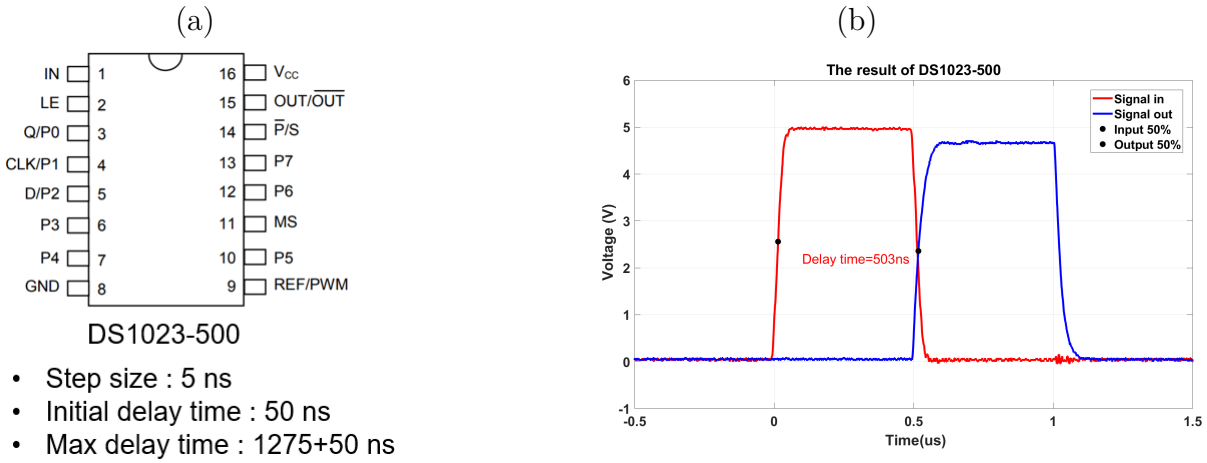

Figure 26: (a) Datasheet of the DS1023-500. (b) The result of the DS1023-500.

Figure 27 is the result of the negative high voltage pulse. The negative pulse generator can generate a pulse width from 500 ns to several microseconds with the amplitude as low as -1 kV.

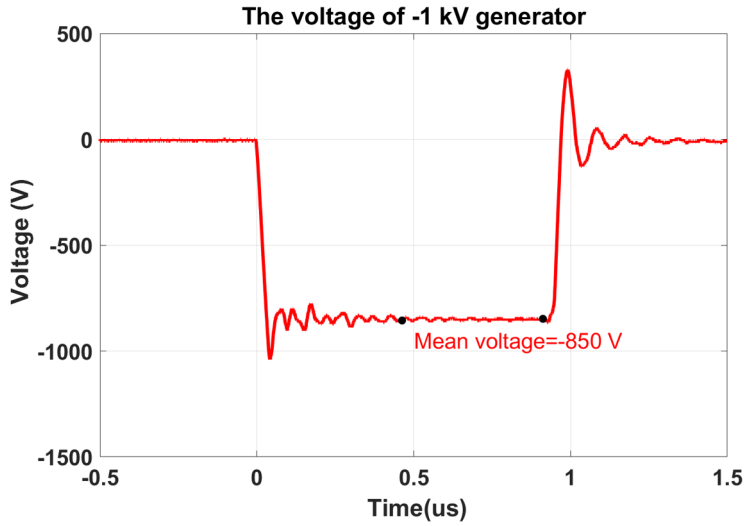

Figure 27: The result of the negative high voltage pulse.

4.2.2 The high-voltage power supply

In the pinhole camera control box, there are two high-voltage power supplies. One provides high voltage to the negative high-voltage pulse generator and the other to MCP set. The output voltage of the high-voltage power supply is controlled by the input analog voltage. The analog voltage is generated by the IC AD7533. The AD7533 converts the binary digital input applied by the Arduino Mega to an analog output. Figure 28 is the relation between the power supply and Arduino.

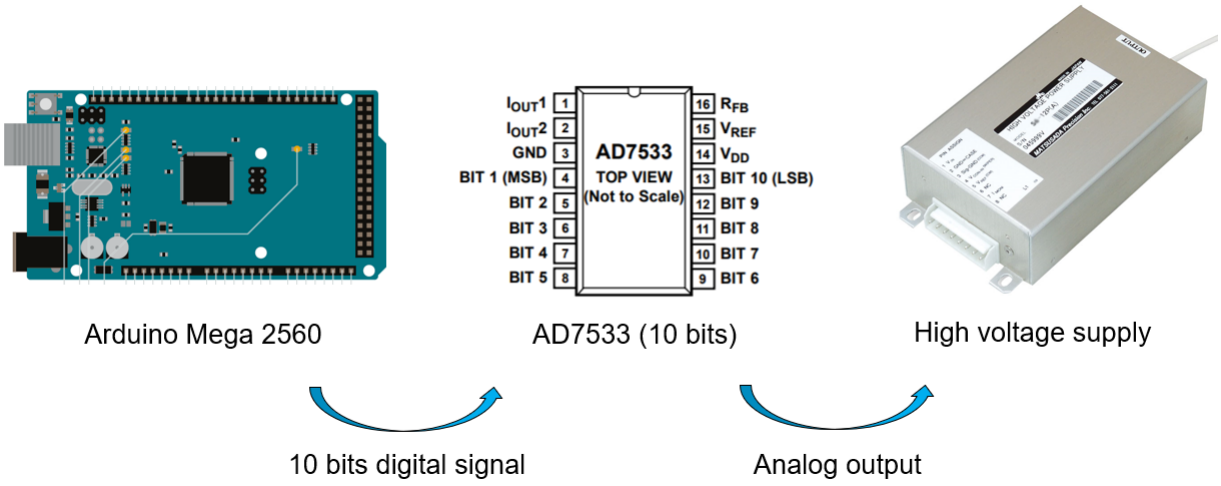

Figure 28: The relation between the power supply and Arduino.

4.2.3 LabVIEW GUI

To control the pinhole camera, we use the LabVIEW GUI to control the Arduino to send the digital signal. The LabView GUI includes : process of connecting with Arduino and CMOS camera, camera setting, high-voltage control, camera trigger, disconnecting the camera and saving the image taken by the camera. Figure 29 is the flowchart for the LabVIEW GUI. Whenever there is an error, the GUI will go back to the initial starts and halt.

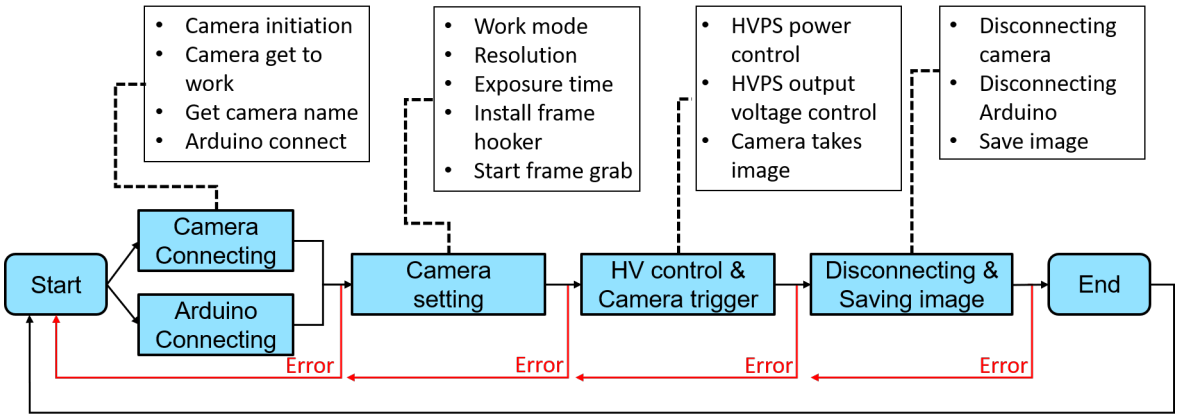

Figure 29: The flowchart for the LabVIEW GUI.

The code of the LabVIEW is in Appendix7.2. The circuit of the pinhole camera control box is in Appendix 7.3. And the circuit layout of the circuit of the pinhole camera control box is in Appendix 7.4.

4.3 Discussion

The pinhole camera has been assembled and installed in the system. The pinhole camera control box has been made and assembled. The LabVIEW GUI to control the control box and CMOS camera was also written. However, the system still has serious problems. The camera couldn't be triggered successfully. The connection between the control box and computer was not stable. When the system was in charging state, the Arduino would disconnect from the computer. When the system discharges, there is a huge EMP in the free space. The EMP would cut the connection between the CMOS camera and the computer. The EMP also shuts down the oscilloscope and the computer. Therefore, we are currently unable to capture photos of the plasma jet by the CMOS camera in the visible-light region and by the pinhole camera in the x-ray region. This technical problem still needs to be resolved in the future.

5 Future work

The pinhole camera has been assembled and installed in the system. However, the camera couldn't successfully be triggered. In the future, we will solve the technical problem of triggering the camera. We will also use the x-ray pinhole camera to take images of the plasma jets in the x-ray region from the side. The physics of the plasma jet generated by the twisted-conical-wire array will be studied by analyzing the image of the plasma jet.

6 Reference

[1] Voltage multiplier. https://upload.wikimedia.org/wikipedia/commons/9/9f/Voltage_amplifier_explain.png.

[2] D. J. Ampleforda, et al., PHYSICS OF PLASMAS 14, 102704 (2007)

[3] D. J. Ampleforda, et al., PRL 100, 035001 (2008)

7 Appendix

7.1 The drawing of the new conical-wire array

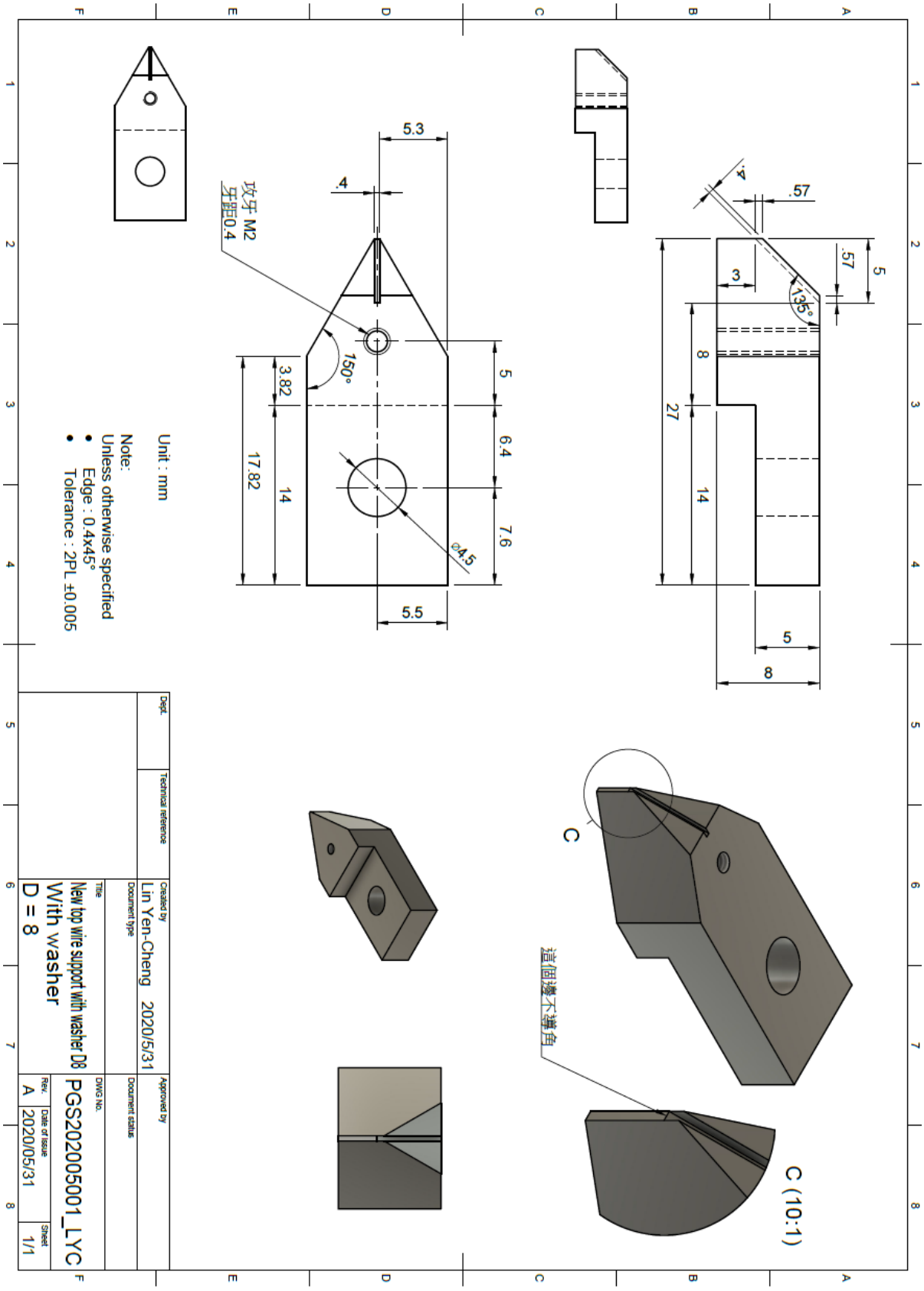

Figure 30: The drawing of the new conical-wire array.

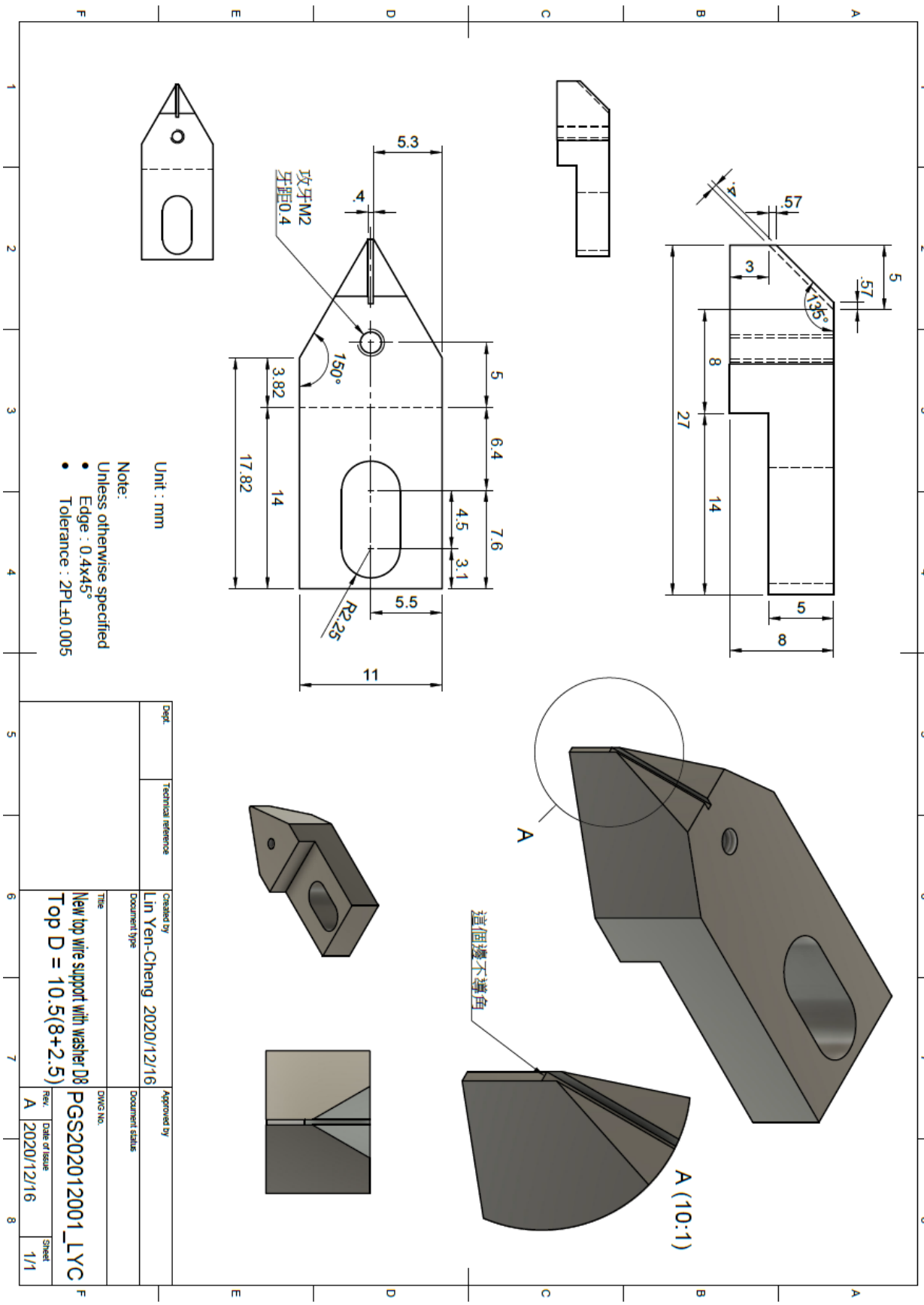

Figure 31: The drawing of the new conical-wire array.

7.2 The code of the LabVIEW

Figure 32: The GUI of the LabVIEW code.

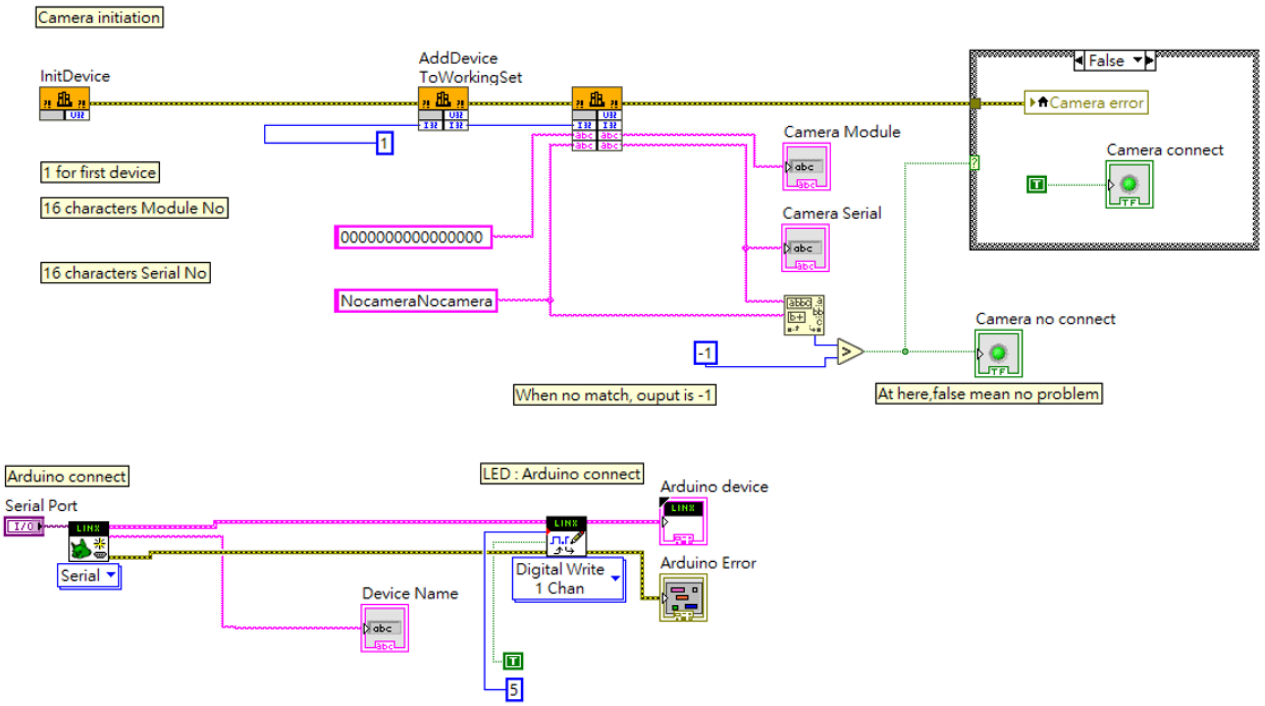

Figure 33: The code of the LabVIEW-connecting.

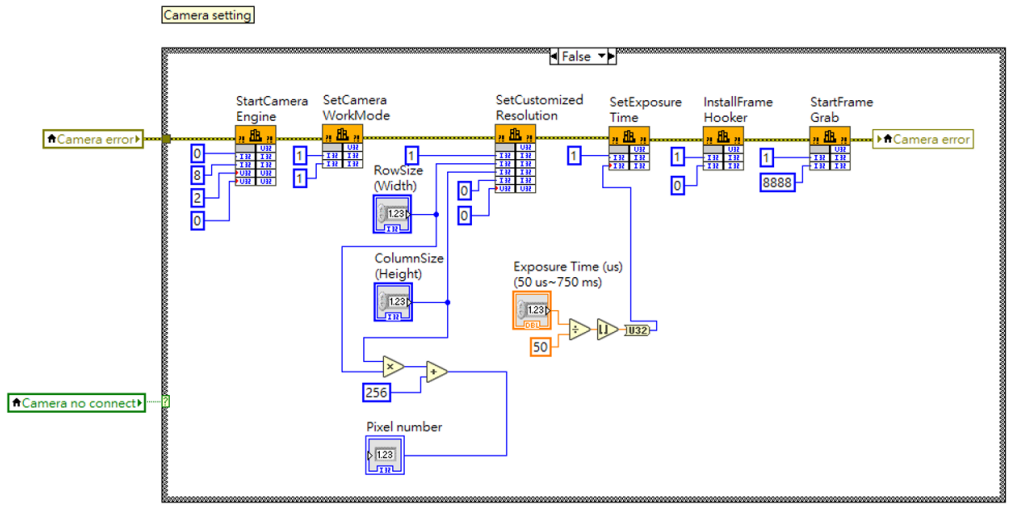

Figure 34: The code of the LabVIEW-camera setting.

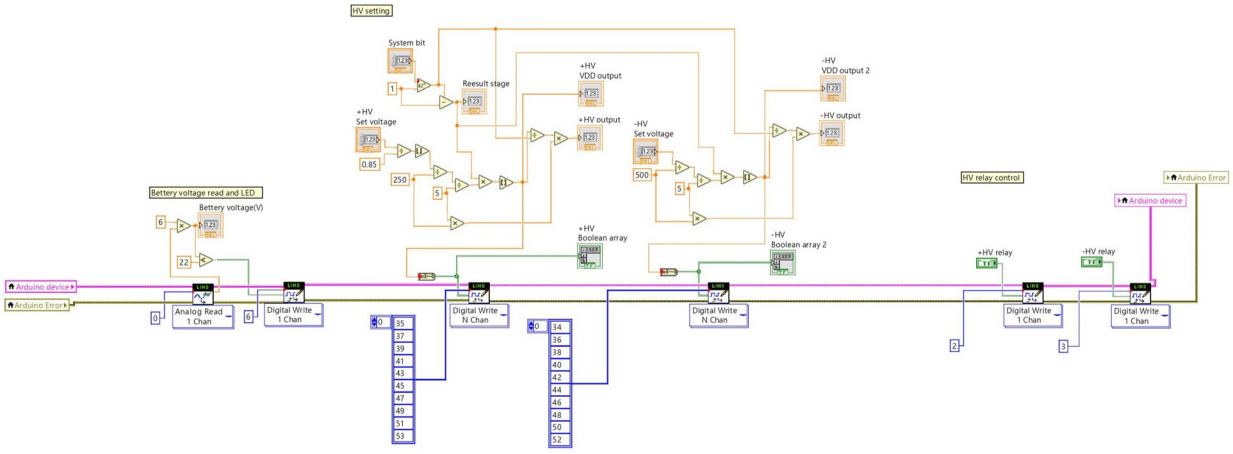

Figure 35: The code of the LabVIEW-HV control.

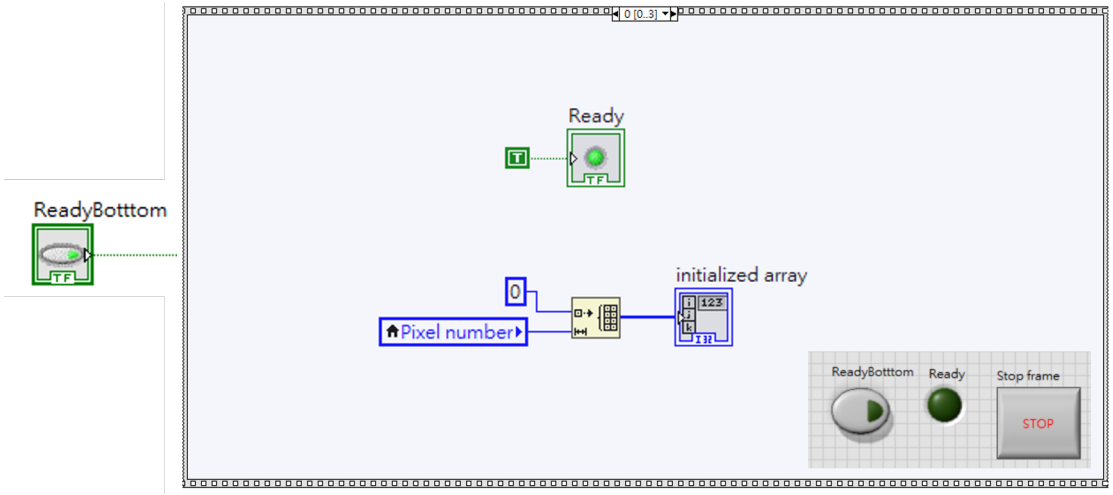

Figure 36: The code of the LabVIEW-Camera trigger 1.

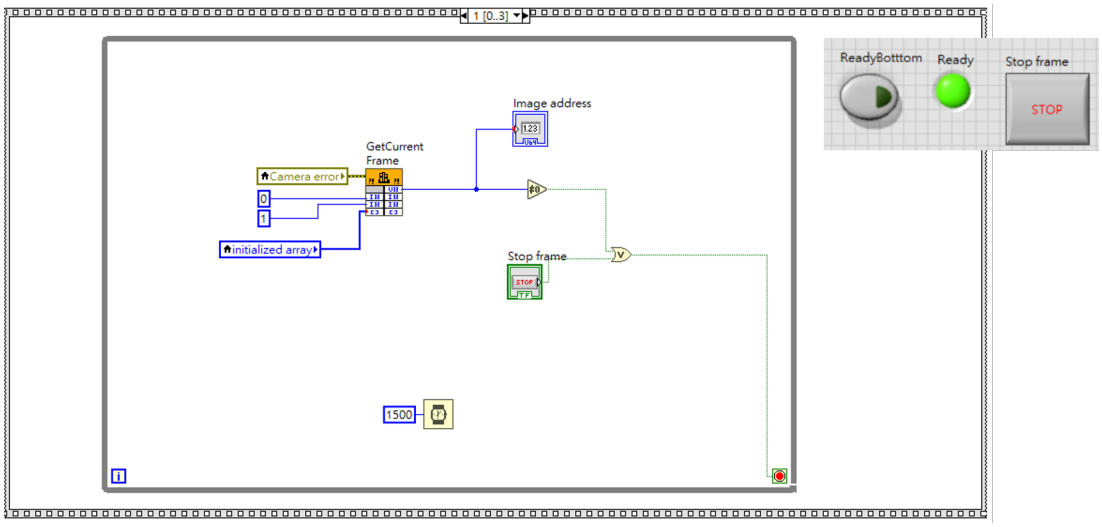

Figure 37: The code of the LabVIEW-Camera trigger 2.

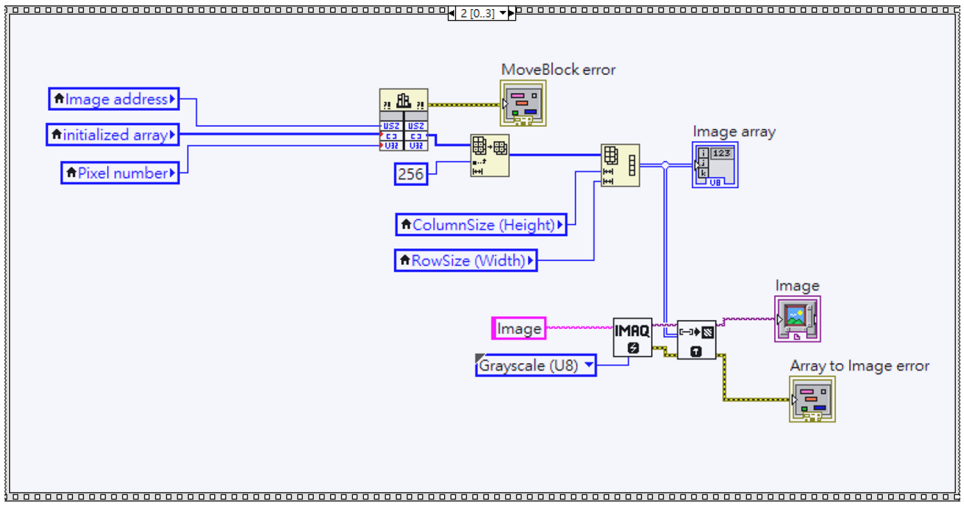

Figure 38: The code of the LabVIEW-Camera trigger 3.

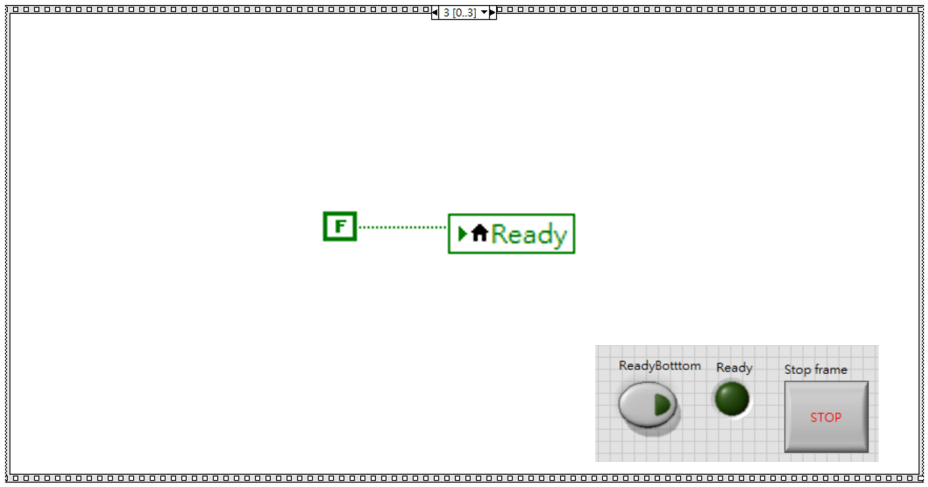

Figure 39: The code of the LabVIEW-Camera trigger 4.

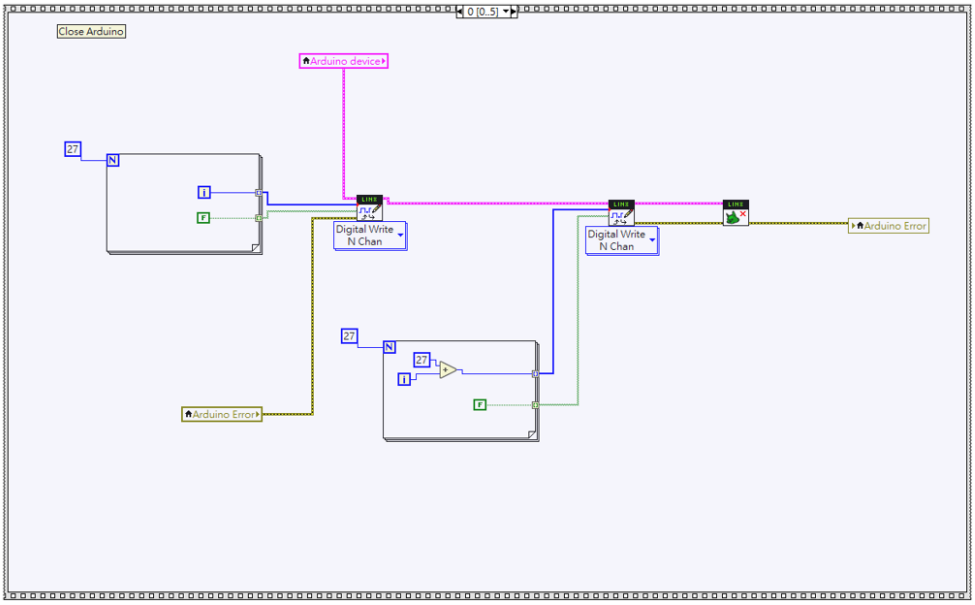

Figure 40: The code of the LabVIEW-Arduino disconnecting.

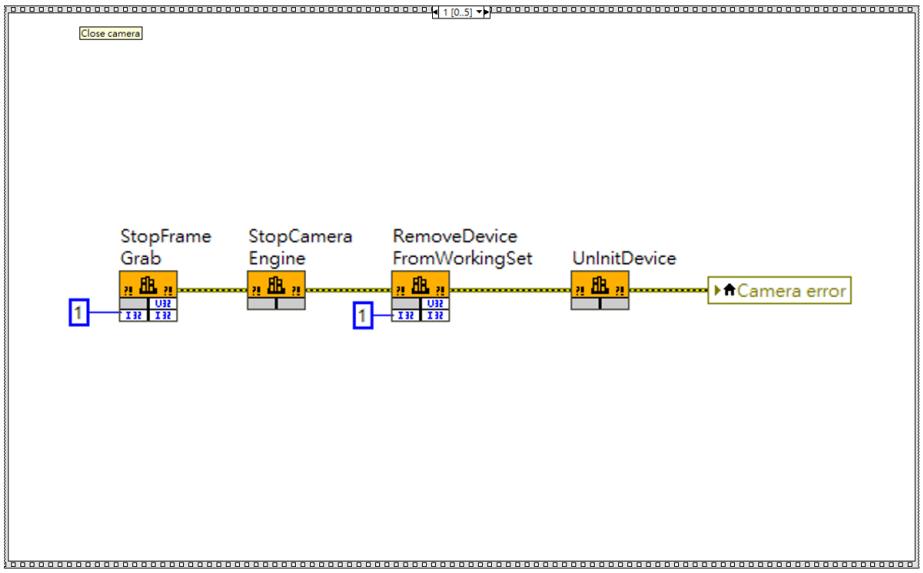

Figure 41: The code of the LabVIEW-Camera disconnecting.

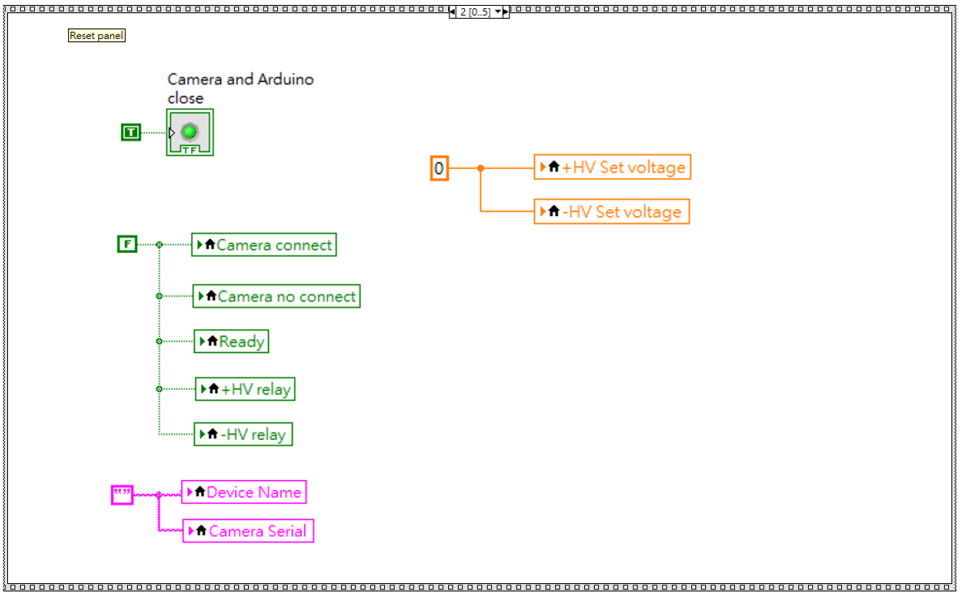

Figure 42: The code of the LabVIEW-Program initialize 1

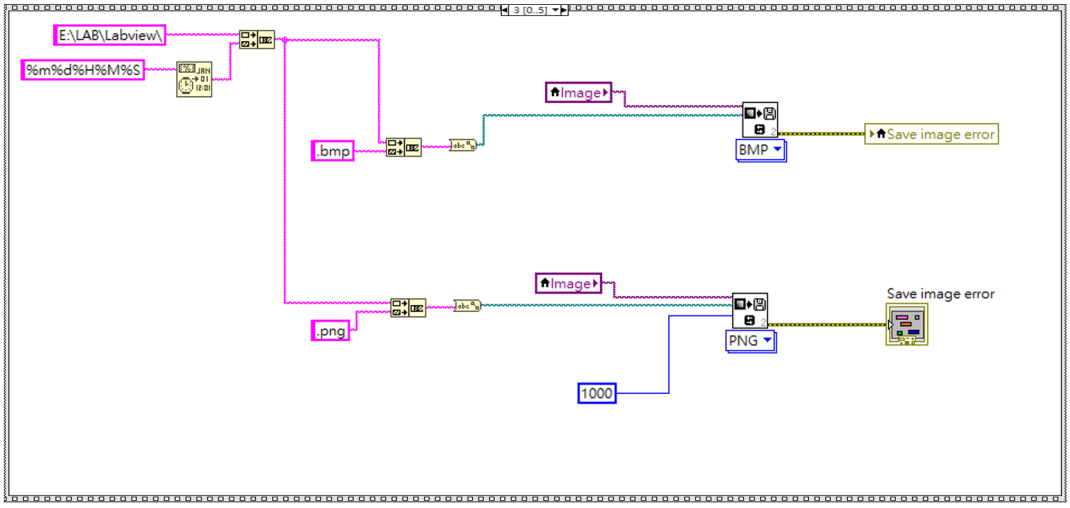

Figure 43: The code of the LabVIEW-Saving image

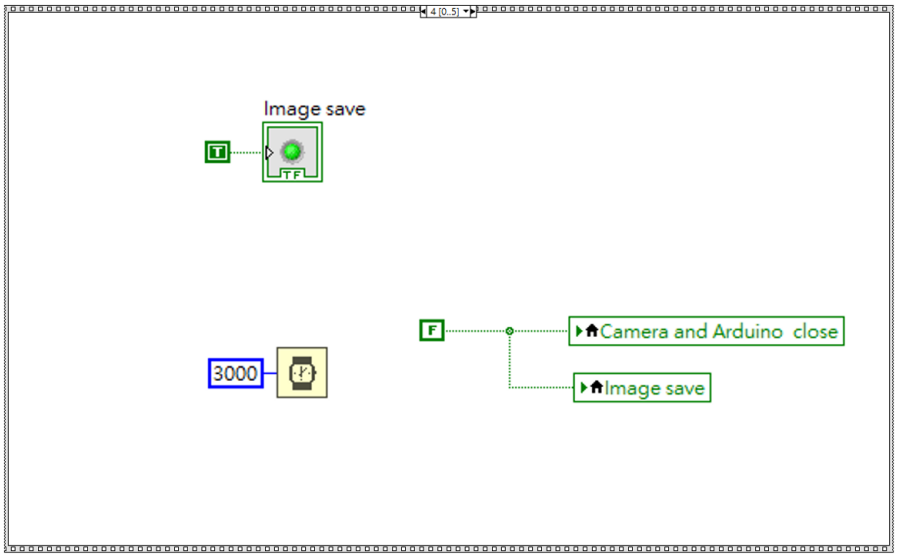

Figure 44: The code of the LabVIEW-Program initialize 2

7.3 The circuit of the pinhole camera control box

7.3.1 Power plate

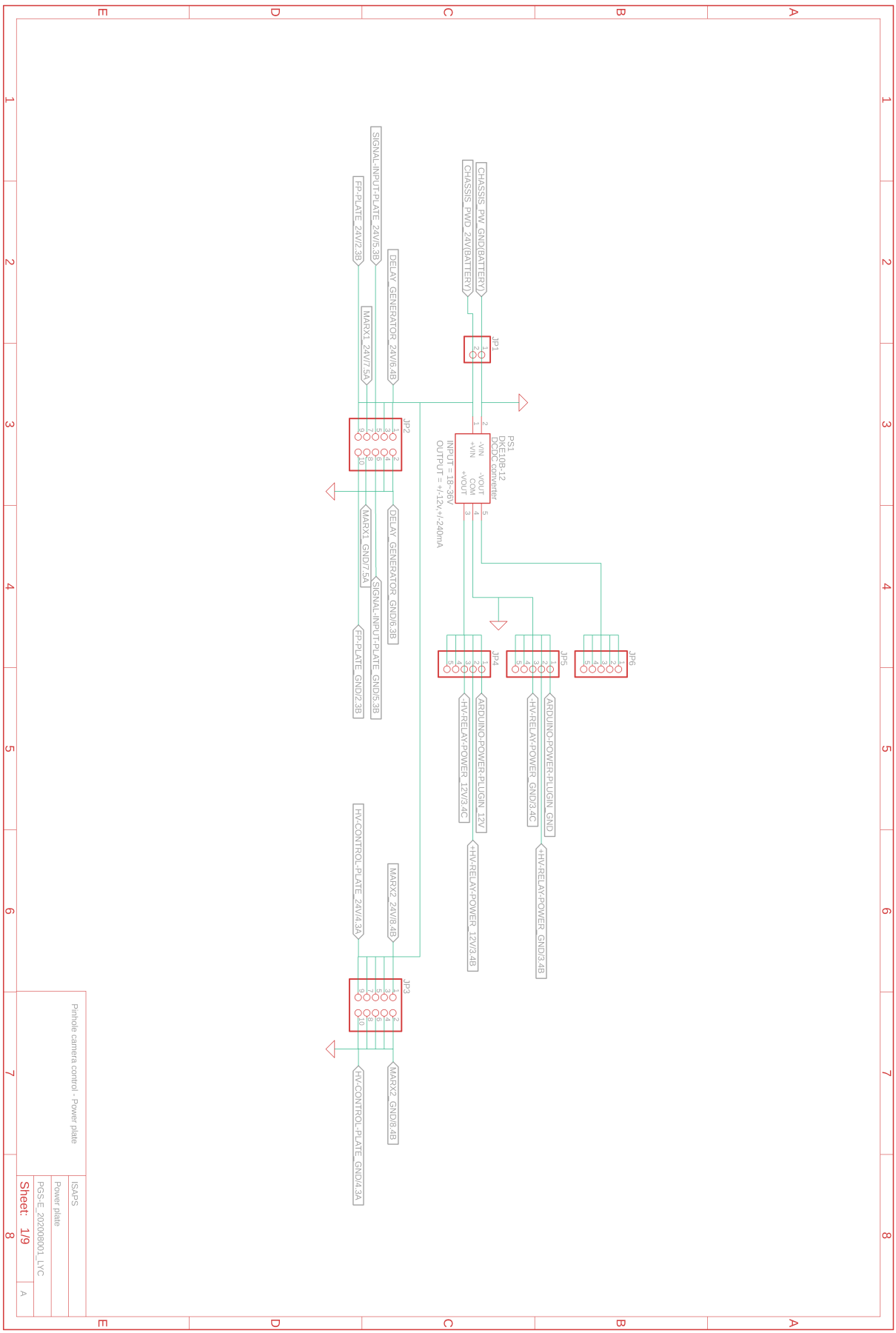

7.3.2 Front panel plate

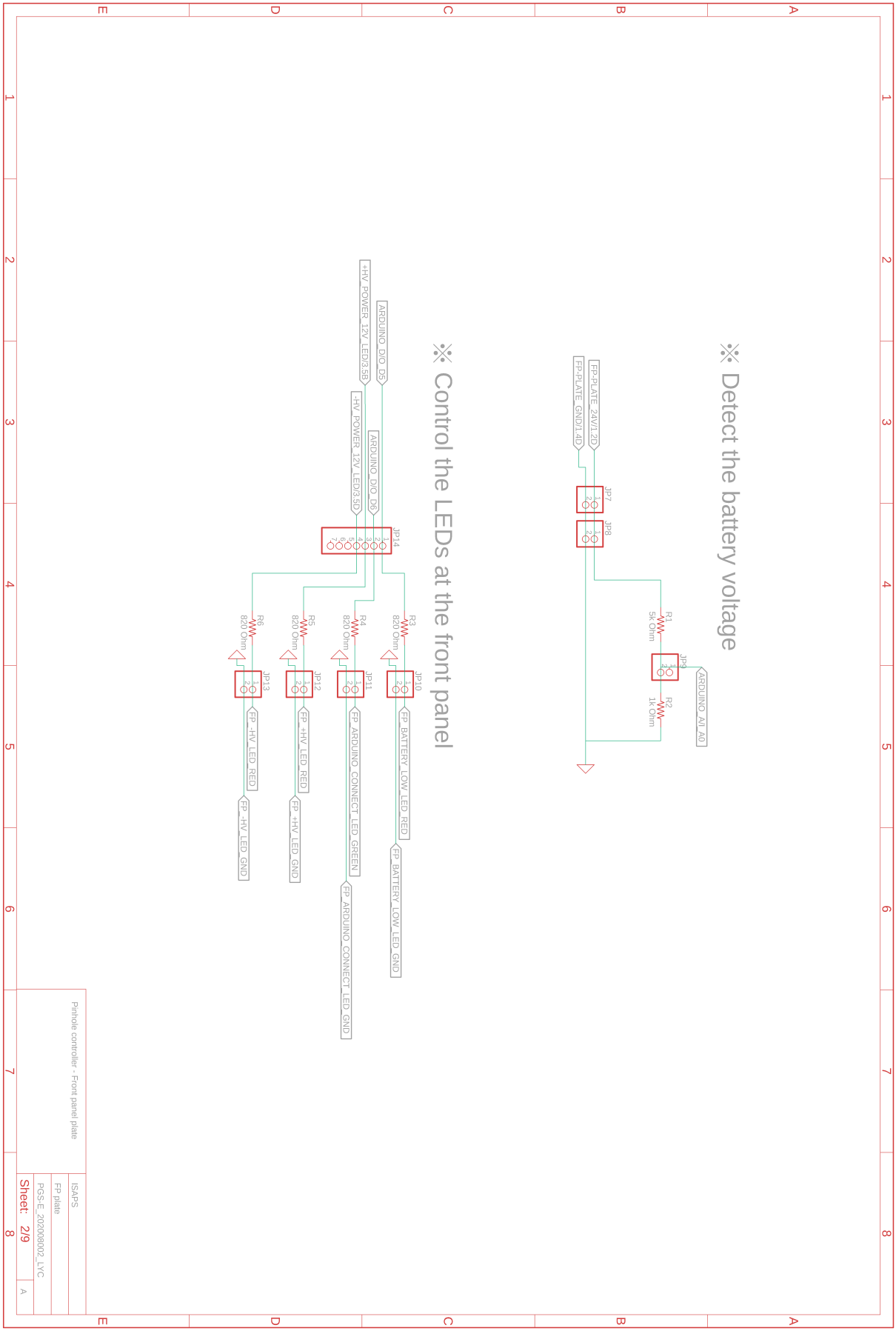

7.3.3 High voltage supply power relay

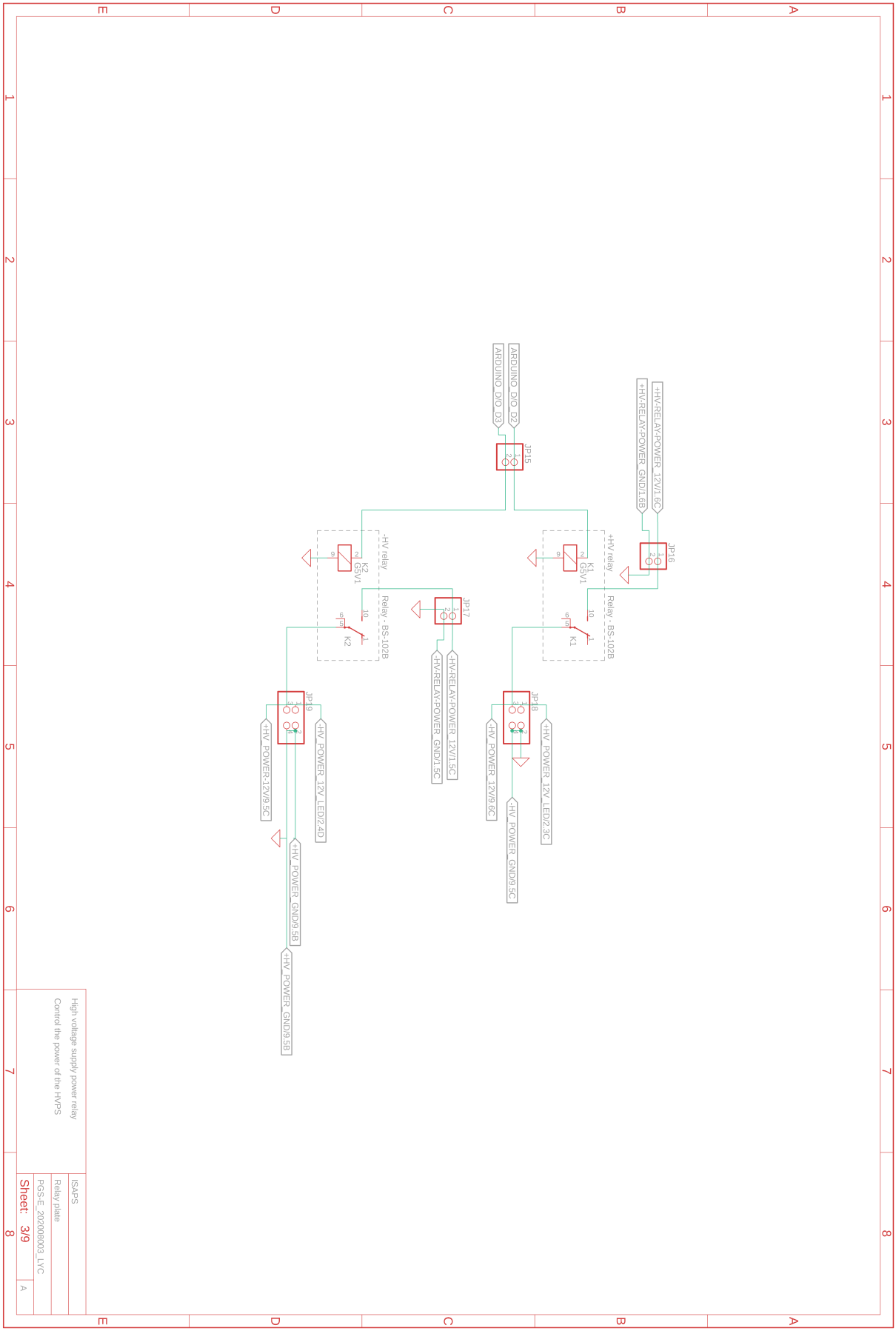

7.3.4 HV control plate

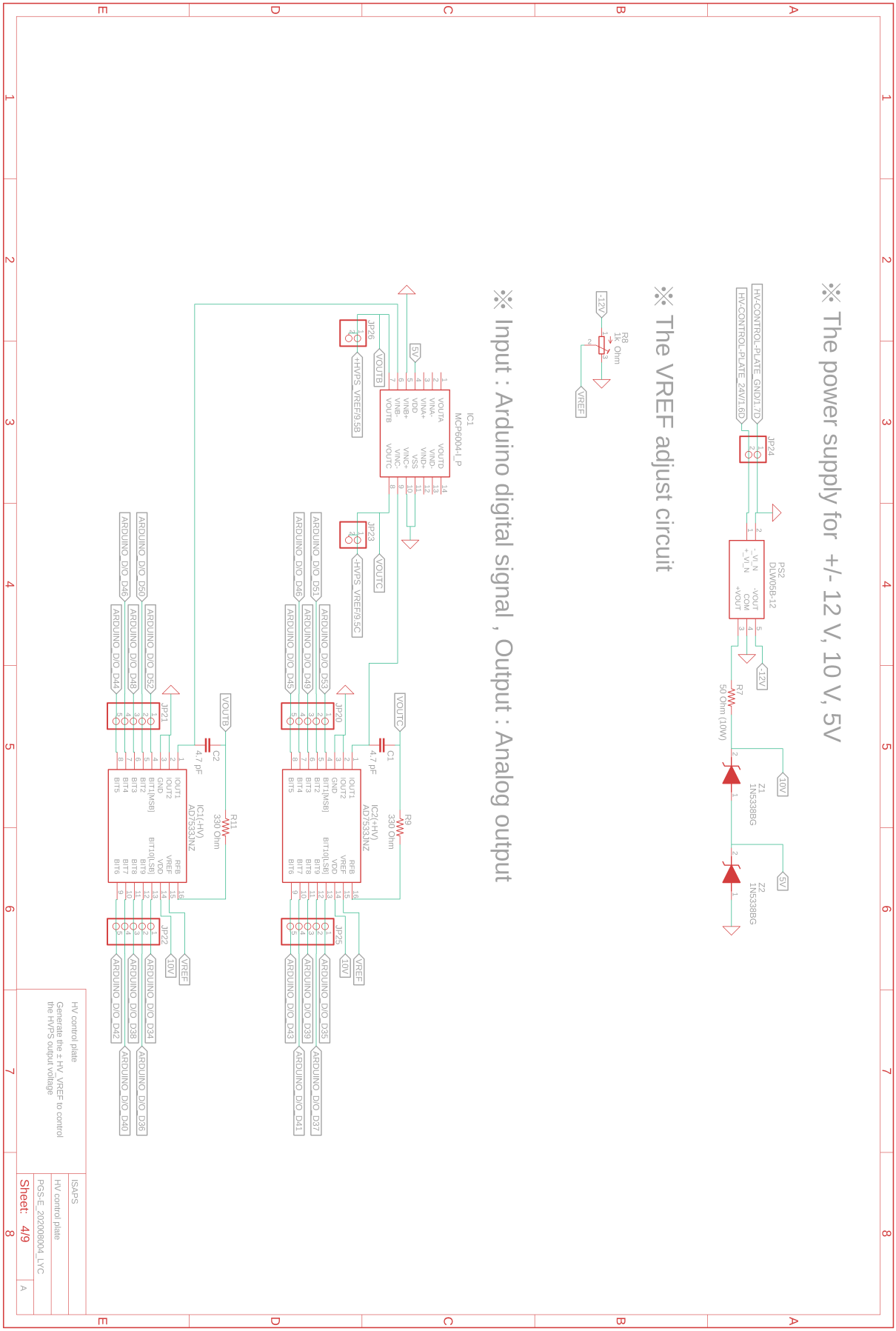

7.3.5 Signal input plate

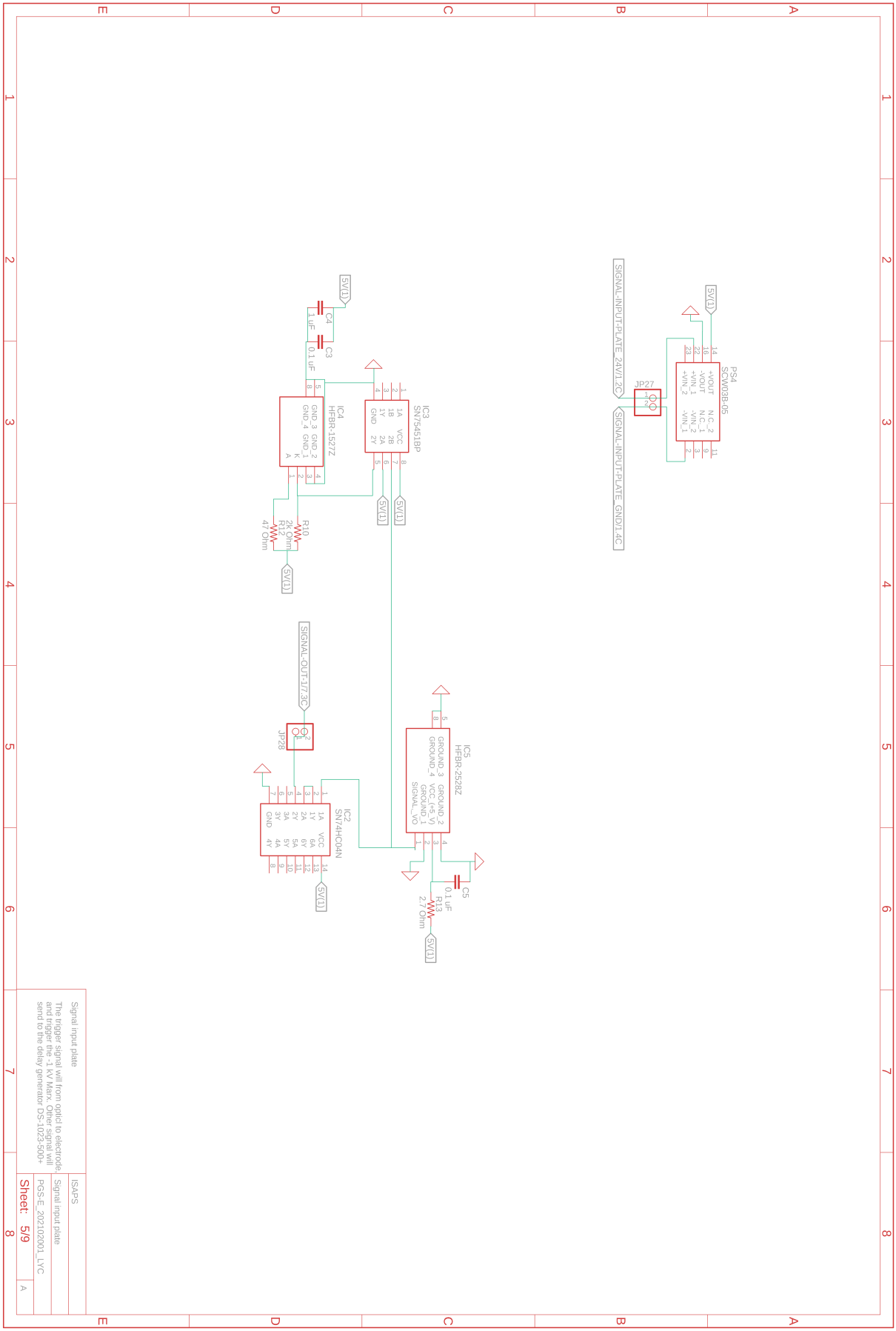

7.3.6 Delay generator - DS1023

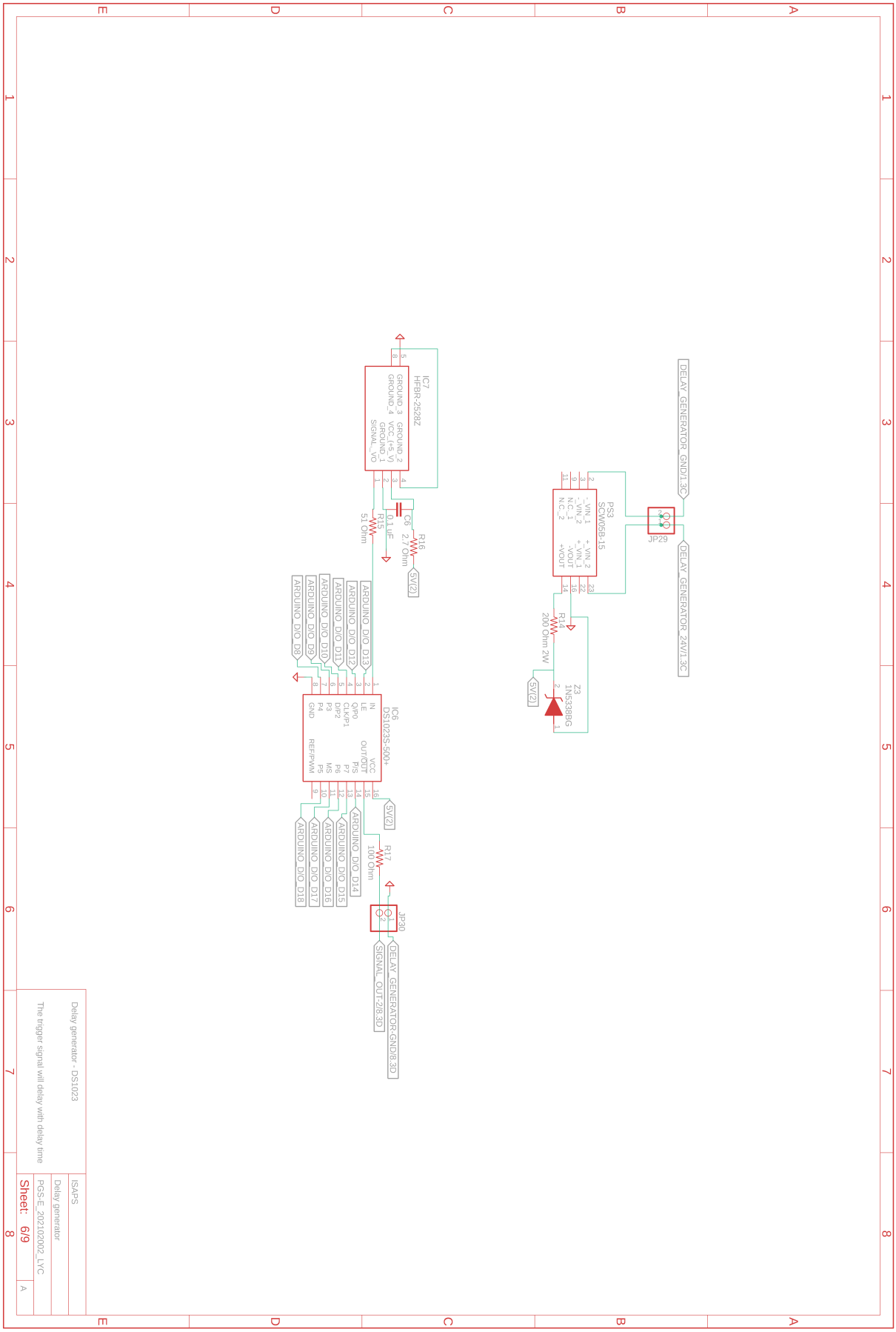

7.3.7 Marx1--1kV generator

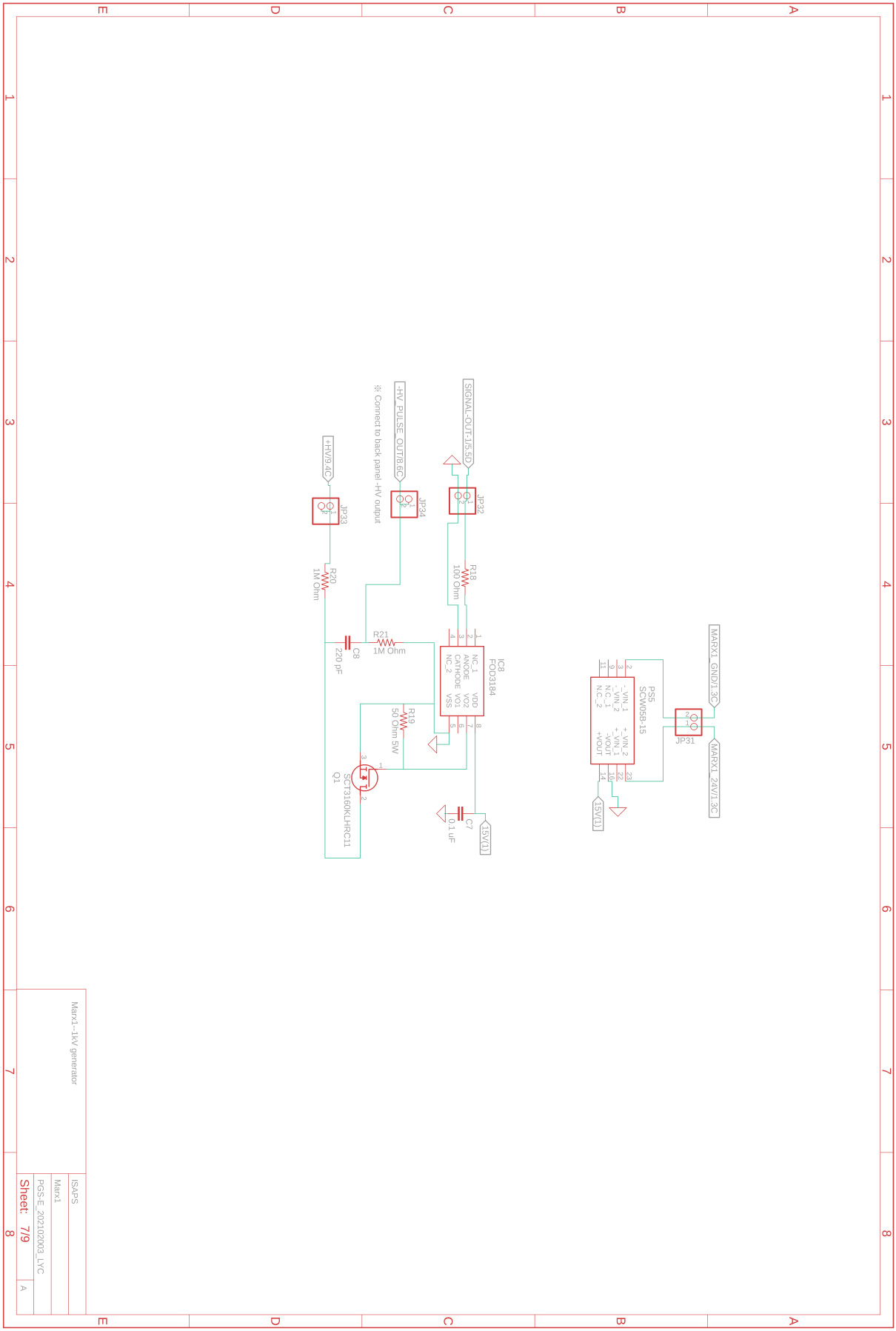

7.3.8 Marx2--dump

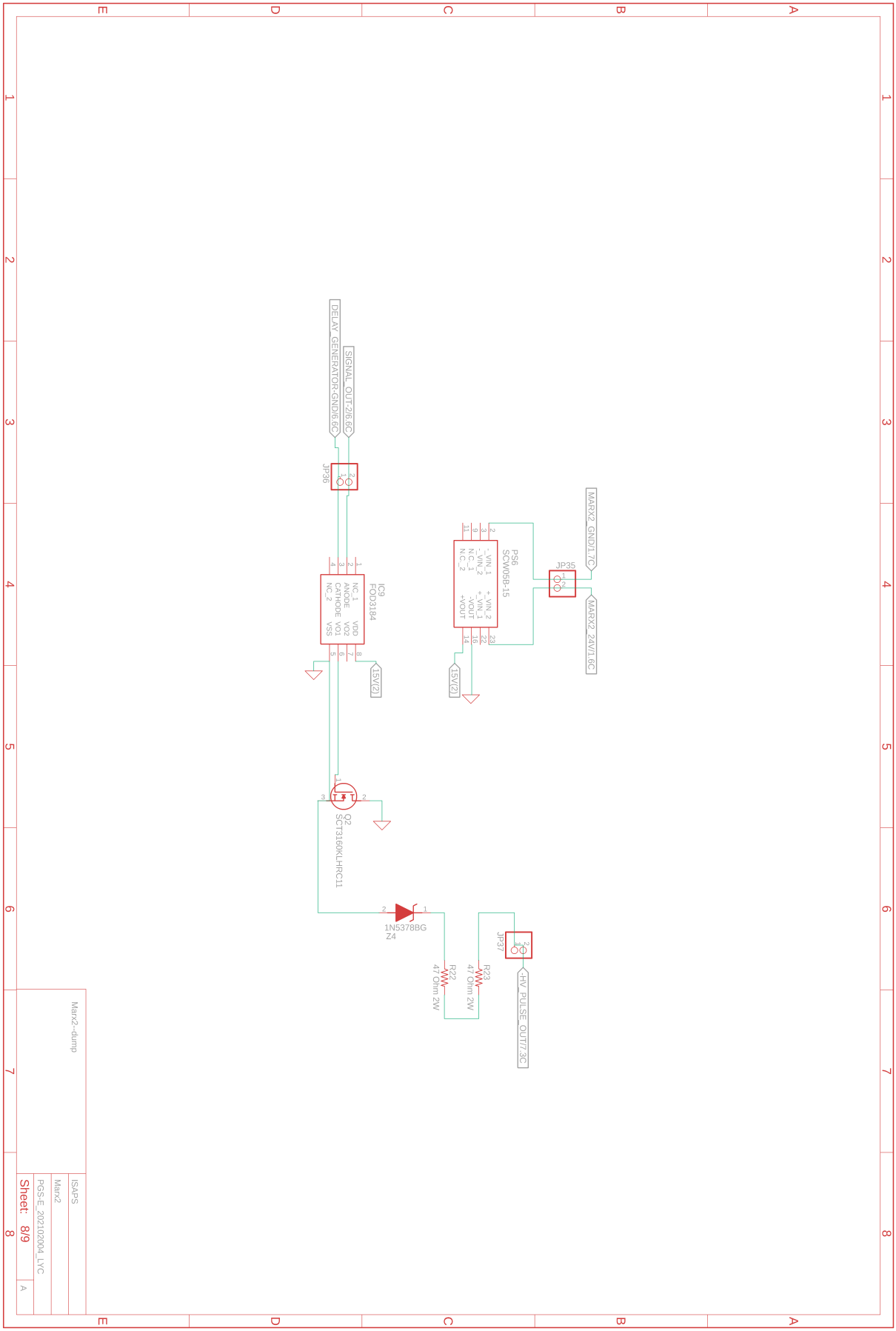

7.3.9 High voltage power supply

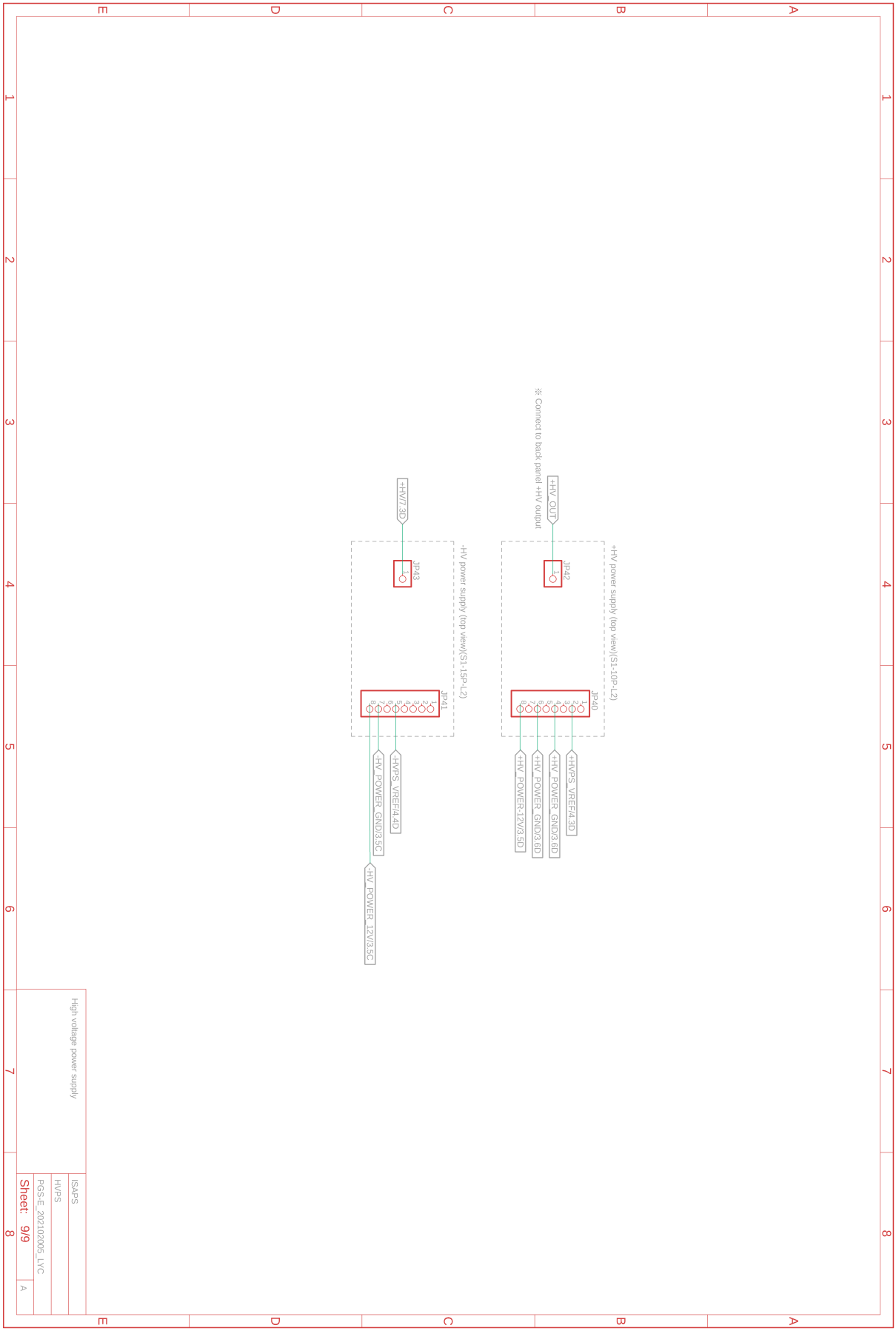

7.4 The layouts of the circuit of the pinhole camera control box

7.4.1 Power plate

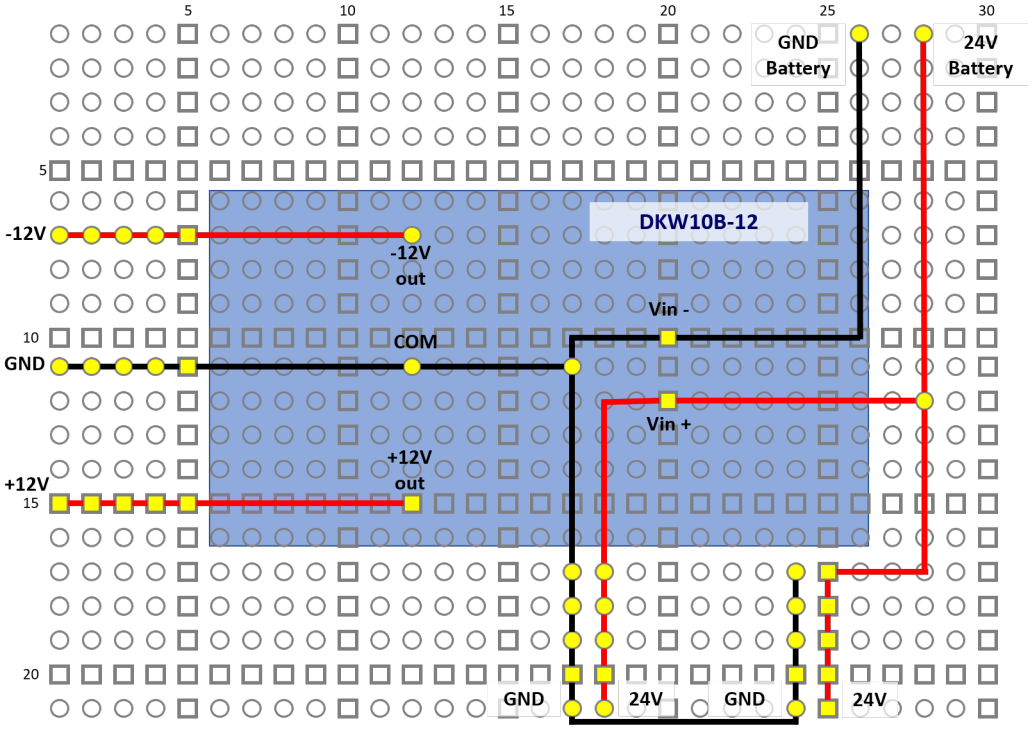

7.4.2 Front panel plate

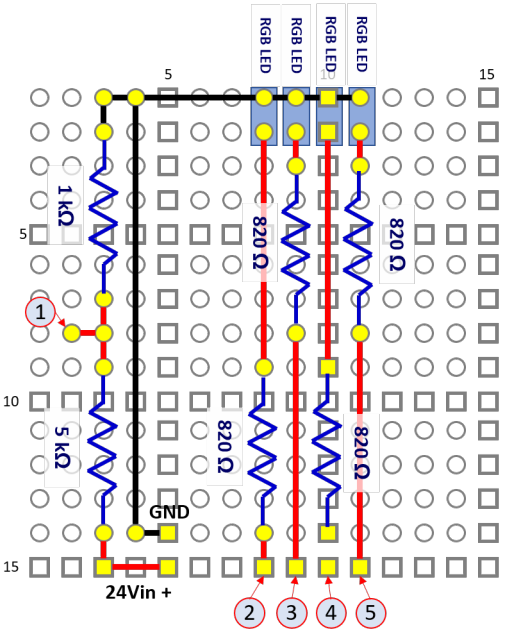

1. Voltage measure : measure the voltage of the 24V battery input voltage(connect to Arduino AO)
2. Battery Low LED control : LED turn on when the voltage of the battery is lower than 22 V (connect to Arduino DO)
3. Arduino ready LED control : LED turn on when the Arduino is turn on (connect to Arduino DO)
4. +HVPS LED control : LED turn on when the +HVPS is turn on.
5. -HVPS LED control : LED turn on when the -HVPS is turn on.

7.4.3 High voltage supply power relay

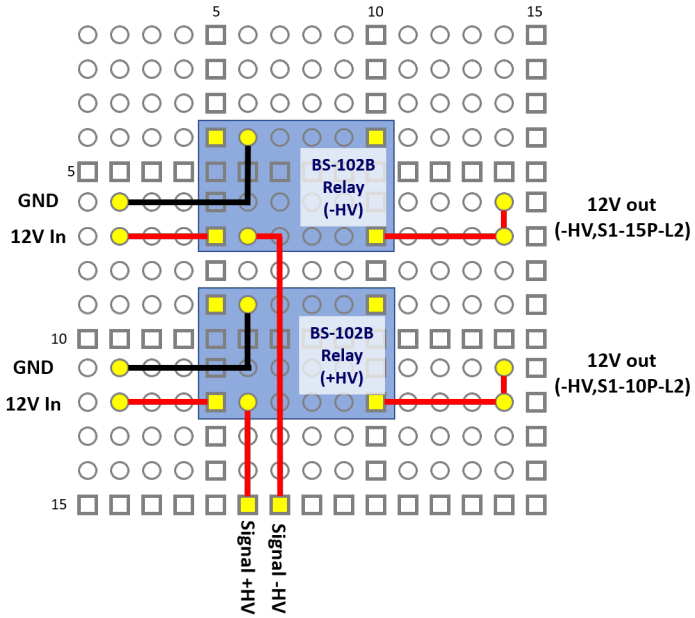

7.4.4 HV control plate

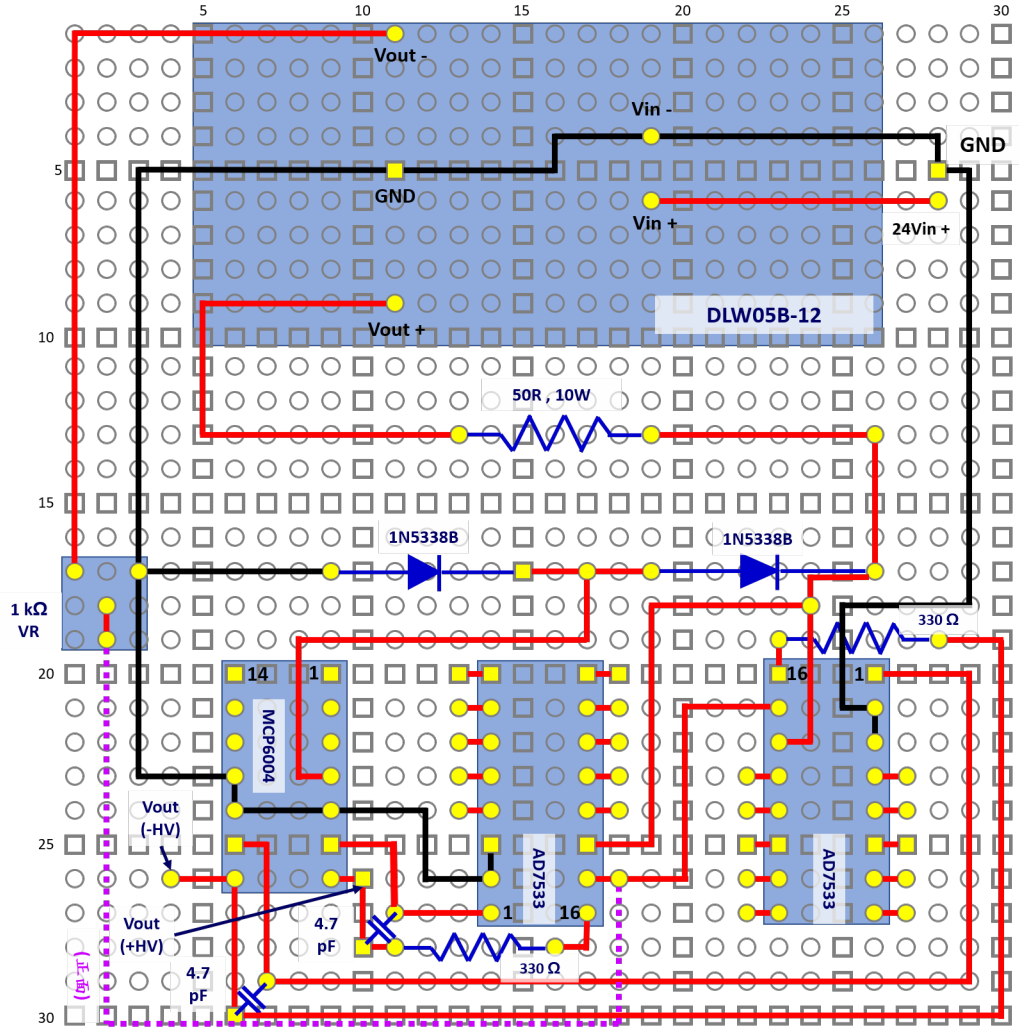

7.4.5 Signal input plate

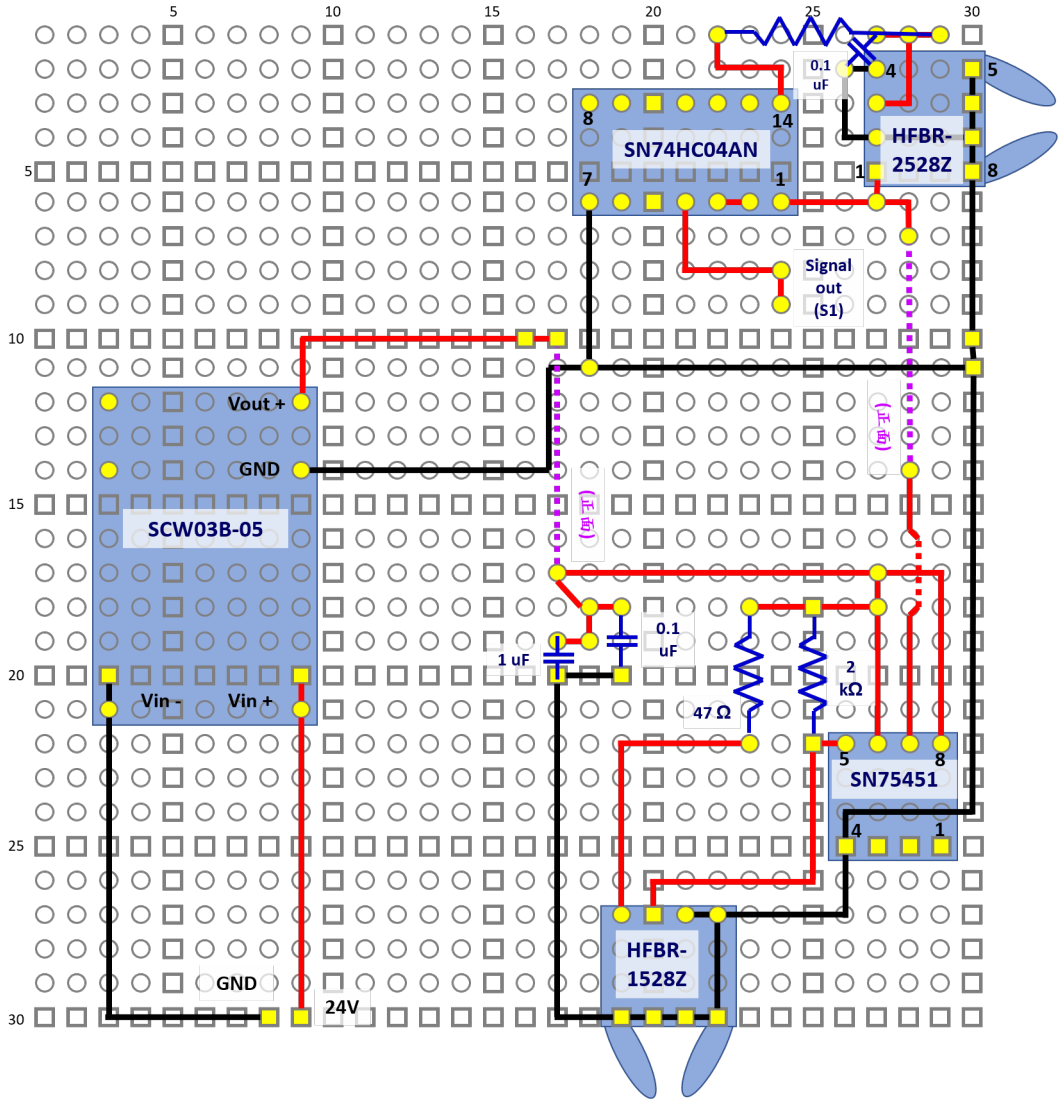

7.4.6 Delay generator - DS1023

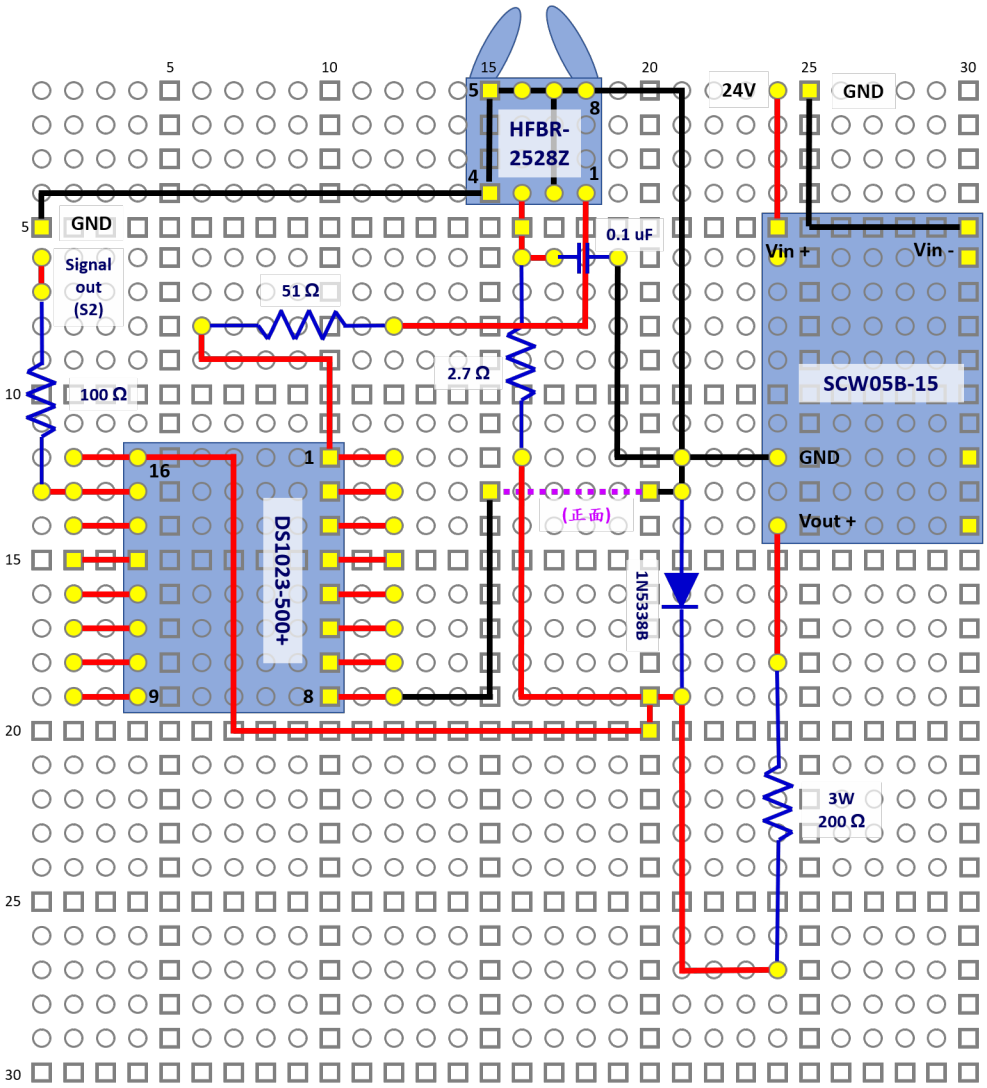

7.4.7 Marx1--1kV generator

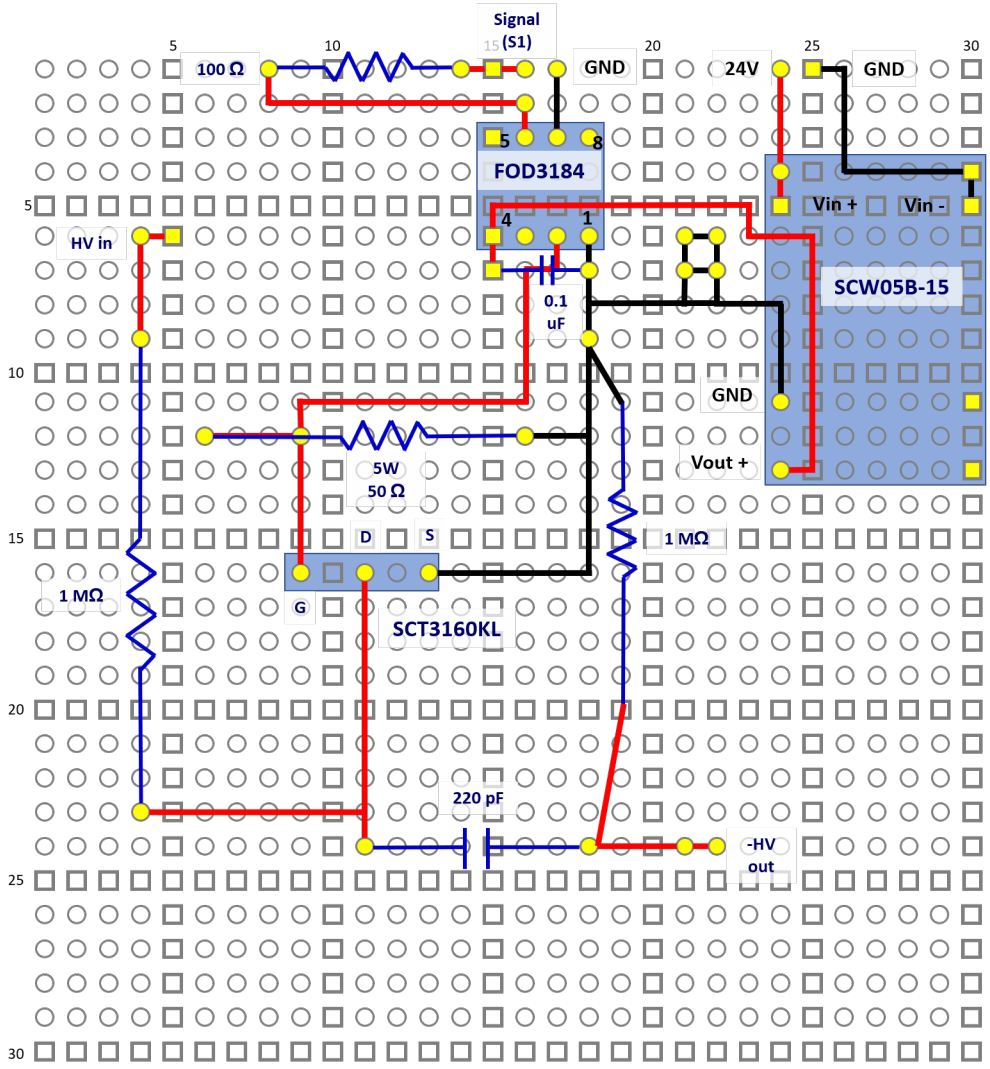

7.4.8 Marx2--dump